Energy & Materials Transition
Princetonlaan 6
3584 CB Utrecht
P.O. Box 80015
3508 TA Utrecht
The Netherlands

www.tno.nl

T +31 88 866 42 56
F +31 88 866 44 75

TNO report

TNO 2023 S11566

Tracing sources of diffuse PFAS contamination in soil near a waste incineration plant

Date	30 June 2023
Author(s)	Noémi Brunschwiler
Number of pages	51 (incl. appendices)
Number of appendices	5
Project name	KARDYSAG-2023
Project number	060.56147

Tracing sources of diffuse PFAS contamination in soil near a waste incineration plant

Noémi Brunschwiler - 7083688 (Utrecht University)
Internal Supervisor: Dr. Thilo Behrends (UU)
External Supervisors: Dr. ir. Joris J. Dijkstra (TNO) & Prof. dr. Jasper Griffioen (TNO and UU)

Summary

Poly- and perfluoroalkyl substances (PFAS), among which are perfluorooctanoic acid (PFOA) and perfluorooctane sulfonate (PFOS), are commonly found contaminants in Dutch soils, often originating from Teflon-producing factories (for PFOA) or firefighting training grounds (for PFOS). An undisturbed area surrounding a waste incineration plant in Alkmaar (Netherlands) was investigated to assess whether the waste incinerator may be a potential source of PFAS to the environment via release through the flue gases. According to the literature, all PFAS compounds should be eliminated during the incineration process. However, the existence of “cold spots” in the oven may result in the survival of PFAS after the combustion. In this study, a total of 10 locations were carefully selected in undisturbed soil profiles composed of loam and clay. Each location was drilled to a maximum depth of 80 cm. Eight of these locations were chosen in the predominant wind direction (from SW to NE) and within a 5 km radius from the waste incinerator in Alkmaar. Two other locations were located upwind and used as “reference” sites for comparison. The samples were analysed for 10 different PFAS compounds and various bulk soil properties were measured including water content, pH, grain size distribution, iron and aluminium oxide content, organic carbon and organic matter content. Based on these properties, the soil sorption coefficient was calculated using different methods found in the existing literature. Hydrus-1D, a reactive transport model code, was used to generate content-depth profiles of PFOA and PFOS under three different deposition scenarios from the waste incinerator to assess whether the emissions from the waste incinerator could account for the observed contamination depth patterns found in the soil samples. The analysis of the results reveals that six of the downwind locations exhibit elevated PFAS content in the top layer of the soil (<30 cm). In high-resolution cores, the PFAS soil profile follows a bell-shaped pattern with the highest content observed at a depth 10-20 cm-bs rather than directly at the surface. This indicates that most of the PFAS contamination originates from past emissions which have now decreased over time. A weak correlation between the distance from the waste incinerator and the measured PFAS content in the soil profile is found. The Hydrus model supports the hypothesis that the observed PFAS content-depth profile can be explained by historical emissions and that the main source of contamination has stopped. Based on the results of this study, a contribution of the waste incinerator to the PFAS contamination observed in the study area is likely, but additional research is needed to investigate the influence of other possible sources.

Contents

1 Introduction

Per- and polyfluoroalkyl substances (PFAS) form a group of synthetic chemicals comprising over 6,000 different chemicals characterized by a complete or partially fluorinated carbon chain of 2 to 16 carbon atoms followed by a functional group (Expertisecentrum PFAS, 2018). PFAS have properties that lower the aqueous surface tension which makes them good surfactants. They are also used for their water- and grease-repellent properties in numerous industries, e.g., paper and food packaging, stain-resistant textile, fire extinguishing foam, Teflon material, non-stick cookware, or coatings (Buck et al., 2011; 3M Company, 1999). Their initial production started in the 1940s, and they have since been used in over 200 applications for various industrial products (ITRC, 2017; Gluge et al., 2020). However, their widespread use is controversial due to their high mobility and recalcitrant behaviour in the environment. A large number of PFAS accumulate in the environment and in living organisms and can be detected in very remote locations such as the Arctic region (e.g., in polar bears) as they can get transported over long distances via the atmosphere and ocean currents (Buck et al., 2011; Expertisecentrum PFAS, 2018; Maddela et al., 2022; Boisvert et al., 2019; Ahrens et al., 2011). PFAS are hence described as “forever chemicals” as they hardly degrade naturally due to the strength and stability of the carbon-fluorine bond which makes them resistant to natural degradation processes (Buck et al., 2011; Solo-Gabriele et al., 2020). They are also considered toxic and health risks for human exposure to PFAS include thyroid diseases, increased cholesterol levels, liver damage, kidney cancer, and developmental effects to unborn children (EEA, 2019).

Long-chain PFAS, defined as PFAS which carbon chain contains >6 C atoms, are the most widely studied PFAS due to their large industrial use and tendency to bioaccumulate (Buck et al., 2011). These substances are all commercially produced and released in the environment during the production, use and disposal of PFAS-containing products. Due to concerns over their long-term health effects and environmental impacts, some long-chain PFAS such as perfluorooctanoic acid (PFOA) and perfluorooctane sulfonate (PFOS) have been regulated by different regulatory agencies in the EU (EU Water Framework Directive) and classified in 2016 for PFOA, resp. 2009 for PFOS, as Persistent Organic Pollutant (POP) under the Stockholm Convention (European Commission, 2020; Maddela et al., 2022). Therefore, their production has been strongly restricted by global manufacturers in the EU and alternatives such as short-chain PFAS have been developed to substitute long-chain PFAS (Buck et al., 2011; European Commission, 2020). In February 2023, the European Chemicals Agency (ECHA) published a proposal to ban all harmful PFAS substances in the EU (ECHA, 2023). More than 100,000 sites are estimated to emit PFAS in Europe (European Commission, 2020).

Among the long-chain PFAS, perfluorooctanoic acid (PFOA) and perfluorooctane sulfonate (PFOS) are the most commonly found PFAS in Dutch soils (Expertisecentrum PFAS, 2018c; RIVM, 2020).

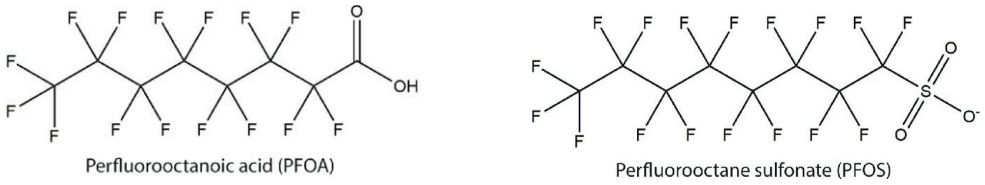

Fig. 1. Structures of PFOA and PFOS (Post et al., 2017).

PFAS do not occur naturally in soil but have become omnipresent as a result of numerous point- and diffuse sources. Therefore, the Dutch National Institute for Public Health and Environment (RIVM) established background values for PFAS content in Dutch soil that aim to prevent further spreading of PFAS from higher contaminated to lower contaminated areas (RIVM, 2020). These background values have been derived from measurements at about 100 locations and represent the background PFAS content that is currently found in soils that are relatively unaffected by human activities (i.e., natural and agricultural areas). The derived values are 1.4 µg/kg of dry soil for PFOS and 1.9 µg/kg for PFOA, respectively (RIVM, 2020). However, soil samples collected around the Netherlands have locally and regionally revealed higher PFAS content in the soil. Groundwater and surface water of the Netherlands also show high concentrations of PFAS (Expertisecentrum PFAS, 2018b, 2018c).

High concentrations of PFAS are mainly found in industrial areas and near firefighting training grounds (Expertisecentrum PFAS, 2018c). PFOA deposition in the Netherlands has been linked to the activity and air emissions of the Chemours/DuPont factory, which produced polytetrafluoroethylene (PTFE), commonly known as Teflon, from 1970 to 2012 from PFOA (RIVM, 2020). Therefore, elevated concentrations in soil have been observed in a 50 km radius from Chemours (RIVM, 2020). The PFOA concentration is especially high in the area downwind from Chemours (Van Bentum et al., 2017) and has been detected in blood of people living near the factory (Van Poll et al., 2017). As for PFOS, they are mainly found near firefighting training grounds, including military bases and civil airports. Up until 2011, most extinguishing foams indeed contained PFOS for its aqueous film properties and resistance to high temperatures (Expertisecentrum PFAS, 2018c). Other sources of PFAS may include leachates from on-site landfills due to the degradation of household products, large fire events, wastewater treatment plants, diffuse contamination from agricultural lands from the use of PFAS-containing fertilizer, atmospheric deposition from waste incinerators, PFAS manufacturing and processing facilities, or background atmospheric deposition from the sea (Expertisecentrum PFAS, 2018c; Röhler et al., 2021; Xiao, 2022).

Gerardu et al. (2023) found elevated contents of PFOA and PFOS in undisturbed soils downwind from the fluoropolymer factory of Chemours/DuPont. However, the authors concluded that PFOS cannot originate from the factory in the extent found, and that the most likely alternative explanation is historic, rather parallel emissions from nearby sources such as waste incinerators (Gerardu et al., 2023). This makes waste incinerators a potential source for PFAS to the environment.

1.1 Waste incinerators & Treatment

There are currently 13 waste incineration plants in the Netherlands. They mainly burn municipal waste (35%), industrial waste (18%), and residues (38%) (Rijkswaterstaat, 2020).

Fig. 2. Waste incinerators in the Netherlands (two of them are located very near to each other and therefore overlapping and not distinguishable on the map).

By burning municipal and industrial waste containing PFAS (e.g., Teflon material, synthetic material, household products), waste incinerators may release PFAS compounds in the flue gases to the atmosphere. As a result, those PFAS compounds may subsequently deposit at the soil surface downwind from the facility via gravity or rain. However, PFAS should not be detectable in modern waste incinerators, as proper combustion for non-hazardous waste requires homogeneous temperatures of at least 850°C and a minimum of 2 seconds residence time with the presence of 6% oxygen in the post-combustion zone which should fully degrade all PFAS compounds and other persistent organic pollutants (POPs) according to the EU Directive on Industrial Emissions (Taylor et al., 2014; Bakker et al., 2021).

Various studies have yielded different findings regarding the optimal temperature required for the degradation of PFAS. Yamada & Taylor (2003) showed that PFOS were thermally converted at 450°C and highly degraded at 600°C, whereas PFOA degrade at lower temperatures, around 300 to 350°C (Kruisic and Roe, 2004; Kruisic et al., 2005). Xiao et al. (2020) concluded that all PFAS should be near complete decomposition at temperatures reaching 700°C. PTFE (or Teflon) has a complete thermal decomposition at 800°C. Other studies require temperatures of 1000°C to reach full thermal oxidation of PFOS and PFOA (Winchell et al., 2020). During incomplete combustion, long-chain PFAS can break down into smaller PFAS compounds, known as short-chain perfluoroalkyl acids PFAAs, which require even higher temperatures to be degraded (EPA, 2020; Horst et al., 2020). A large number of incomplete combustion products are still unidentified and many combustion by-products unknown (Longendyke et al., 2022).

Furthermore, there are often high fluctuations of temperature and oxygen levels in the post-combustion zone which lead to the creation of “cold spots”. The existence of “cold spots” in the oven is evidenced by the presence of considerable amounts of unburnt natural organic matter in the ashes of waste incinerators (Meima et al., 1999; Ferrari et al., 2002; Van Zomeren & Comans, 2004, 2009). Hence, fire-resistant organic pollutants may possibly survive the incineration process due to heterogeneous conditions in the post-combustion zone in temperature, time or mixing and not complying to modern waste incineration processes standards (EPA, 2020). Partial organic combustion is also enhanced by the presence of catalytic surfaces (EPA, 2020). If PFAS can survive the incineration process, it is possible that they could be detected near waste incineration plants through release in the flue gases.

Until now, the incineration of PTFE (Teflon) has generally been recognized as an insignificant source of PFAS within flue gases. This is primarily attributed to the implementation of best available technologies in incineration plants, where PTFE is expected to undergo complete conversion into hydrogen fluoride (HF) (Aleksandrov, 2019). Other studies, such as the ones from Taylor et al. (2014) or Yamada et al. (2005), show that combustion of fluorotelomer-based polymers does not form detectable levels of PFOA and should therefore not be expected to be a source of PFOA. However, these studies were mostly done under laboratory conditions imitating typical combustion in incinerators. The small-scale reach of these experiments may not be representative for large-scale combustion facilities and neglect uncertainties due to the large diversity of PFAS compounds and behaviours during thermal treatment (Longendyke et al., 2022).

Limited research has been conducted directly on incineration plants regarding the emissions of PFAS in flue gases and ash. A study conducted by Sandblom (2014) in four different Swedish incineration plants concluded that flue gases in waste incinerators from Sweden are not a significant source of PFAAs (among which are PFOA) to the atmosphere. Liu et al. (2021) also investigated three Chinese incineration plants and found low levels of PFAS in both fly ash and bottom ash from these plants. Residues such as PFOS were predominant in fly ash, whereas short-chain PFAS were primarily found in leachates, but China uses large amounts of PFAS-containing products compared to Europe (Liu et al., 2021). These findings suggest that high-temperature incineration processes effectively facilitated the destruction of a majority of PFAS compounds. However, no study was based on direct samples from exhaust fumes from incineration plants, as no suitable measurement method has yet been developed to detect PFAS in flue gases (Sandblom, 2014; EPA, 2020). PFAS concentration in flue gases (and other waste streams) are thus lacking in many studies although quantification would be essential to understand the fate of PFAS (Awad et al., 2021). Therefore, it cannot be ruled out that some PFAS might escape through flue gases during incineration although in theory they should not be detectable after thermal degradation (Bakker et al., 2021).

Furthermore, the historical operation of waste incinerators may differ from the current best practice, so it is very likely that historical emissions of waste incinerators could still be detected in the soil. Therefore, PFAS could be seen in soil profiles due to the historical emissions of old waste incineration plants if vertical transport rate did not wash them away.

1.2 Research question

The aim of this study is to investigate the origin of diffuse PFAS contamination found in Dutch soils and whether waste incineration plants could possibly be (or have been) a significant source of PFAS in the Netherlands via atmospheric deposition. This study will therefore improve understanding of the fate and environmental origin of PFAS. The main focus of this study is on PFOA and PFOS, being the dominant PFAS compounds in Dutch soils. The research questions are the following:

1. Can the PFAS deposition profile be linked to the historical activity of waste incineration plants?

    1.1 Do the ashes of waste incinerators contain PFAS which survived the incineration process?

    1.2 Is there a contrast in the PFAS soil content in the predominant wind direction (SW) from waste incinerators?

    1.3 Is it possible to find a correlation between PFAS and the distance to the waste incinerator?

    1.4 Can the reactive transport model Hydrus-1D be used to model the transport of PFAS in soil profiles, given the possible PFAS atmospheric deposition from waste incinerators?

2. If not, which other possible diffuse sources may contribute to the observed PFAS concentrations?

2 Methods

2.1 Study area

This research took place in Province North Holland, near the Alkmaar waste-to-energy plant. The plant burned about 640,000 tons of waste in 2018, among which 47% were industrial waste, 26% household waste, 24% residual waste and 2% mixed municipal waste (Rijkswaterstaat, 2020). All these types of waste are suspected to contain PFAS. The former incinerator VVI Alkmaar was located 1 km North and was in operation from 1974 to 1996, before being replaced by the current one. The study area was chosen due to the absence of a large industrial area or other potential known PFAS sources, and the relatively inhabited agricultural polder area downwind from the factory. The geology of the region consists mainly of marine loam and clay sediments. Clay and loam have a high sorption capacity and PFAS are, therefore, expected to accumulate in the top and infiltrate slower than in sandy soils.

2.2 Sampling

Preferably, sampling sites were selected in areas that were as undisturbed as possible. To select sampling locations, historical and geological maps were checked to avoid land where ploughing took place (for instance for agricultural practice), which would disturb the top layer of the soil. Another source of disturbance is the presence of gas pipes. Residential areas also undergo a lot of construction work (and hence soil mixing) and have increased diffuse PFAS contamination from human activities and were therefore avoided as much as possible. Private landowners were asked to point out locations where disturbance had been minimal over the past 4 to 5 decades, and for permission to take samples on their land. The predominant wind in the area was checked on KNMI and its direction is South-West (i.e., the plume runs to North-East), so we can separate samples in “downwind” (where high PFAS content is expected) and “reference” (where background values are expected) locations from the waste incinerator chimney.

Based on Mennen et al. (2010) who investigated dioxine contamination, the maximal deposition around a waste incinerator is expected to be within 1 to 2 km from the plant, and decreases quickly afterwards, so no high PFAS concentration would be expected at a distance larger than a few kilometres from the plant. Another RIVM report (1989) stated that emission of compounds (including fluorine compounds) from waste incinerators are most likely to deposit within 2 km from the source (with some extended tailing up to about 10 km but with much lower deposition). We, therefore, hypothesized that deposition of PFAS occurs at similar distances.

To verify the hypothesis that waste incinerators are a diffuse source of PFAS, soil samples were collected near the Alkmaar waste incinerator, in the primary wind flow direction (North-eastern plume) and at increasing distances from the plant (within a radius of 5 km). Locations were selected at which the soil profile was “undisturbed” (no tillage) for at least 50 years, i.e., since the commissioning of the old waste incinerator (VVI Alkmaar; 1974). To find undisturbed locations, historical maps were consulted (topotijdreis.nl) and information was obtained from local farmers and land owners. Furthermore, sites with homogeneous soil, vertical infiltration of precipitation

and no seepage of groundwater were preferred. The selected sites are described below.

The sampling campaign took place on the 27th of January and 4th of February 2022. 10 locations were investigated, and 38 samples collected using an Edelman auger (Ø 7cm) and a 2 m gauge, in the same manner as described in Gerardu et al. (2023). Eight locations are situated downwind of the incinerator and within a 5 km radius of the plant, and 2 locations were used as a “background” measure and taken upwind the waste incinerator for reference, as shown in Figure 3. The samples all consist of marine clay sediments.

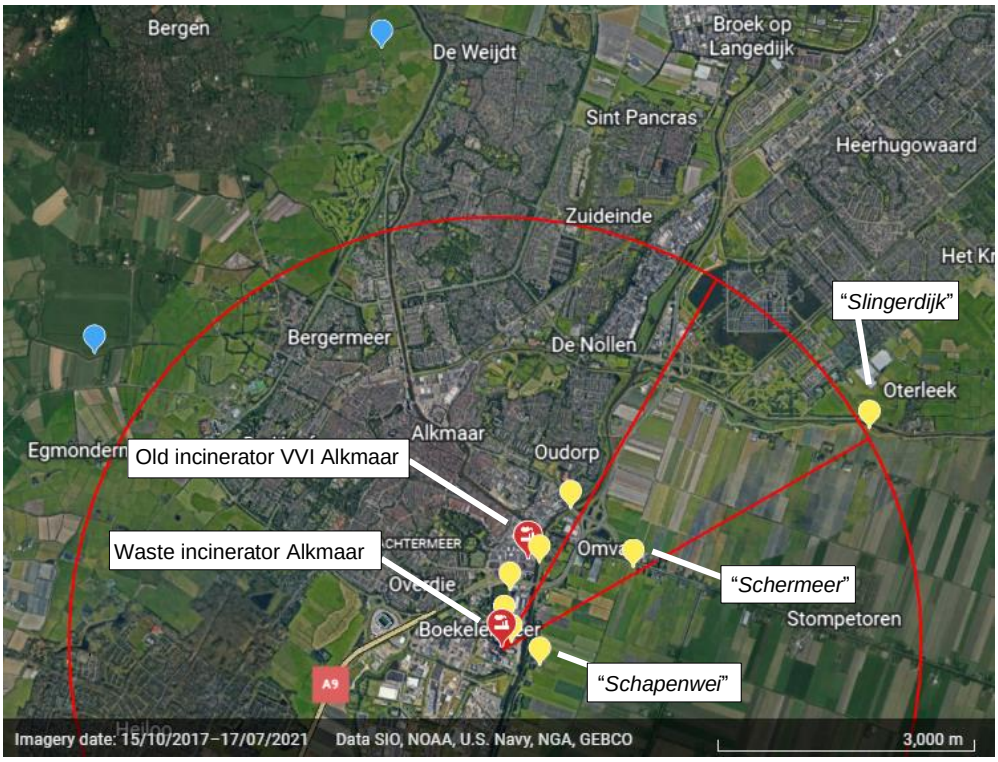

Fig. 3. Sampling locations. In yellow are downwind locations, in blue upwind (reference) locations. The red circle shows a radius of 5 km around the new waste incinerator and the lines show the NE wind direction.

Previous research on PFAS by Gerardu et al. (2023) has shown that topsoil layers are enriched with PFAS while bottom soil layers (i.e., up to 3 m-bs) contain low to undetectable amounts of PFAS. Considering that clay and loam soils presumably have a higher sorption capacity for PFAS than the sandy soils of Gerardu et al. (2023), and that the groundwater table is relatively shallow (~1 m), the samples were collected down to a depth of 80 cm-bs (after which no PFAS were expected). Two locations in NE direction (referred as *Schermeer* and *Schapenwei*) were sampled at high resolution in intervals of 10 cm down to 80 cm-bs. These locations were undisturbed (for ~400 and ~60 years respectively, as estimated by the landowners) and therefore suitable for a high-resolution core. The location in NE direction *Slingerdijk* (the old dike around the polder) is presumably also undisturbed, but 5 km away from the incinerator and therefore presumably less contaminated. This location was sampled down to 40 cm depth. The locations in NNE direction were in urban areas hence disturbance cannot be excluded, although the historical maps do not

show clear interventions. There, most samples were taken at a shallow depth (i.e., up to 40 cm-bs), with 2 to 4 samples collected per location.

Table 1. Sampling locations.

#	Name of location	Rounded coordinates	Number of samples	Depth to depth interval [cm]
1	Slingerdijk	4.826, 52.633	2	0-40
2	Schermeer 1633	4.785, 52.618	9	0-80
3	Schapenwei	4.769, 52.607	8	0-80
4	Laanenderweg	4.764, 52.610	2	0-30
5	Sandpit South	4.763, 52.612	2	0-30
6	Sandpit North	4.764, 52.616	2	0-30
7	Omval South	4.769, 52.619	4	0-40
8	Omval North	4.775, 52.624	2	0-30
9	Reference Bergen	4.692, 52.641	4	0-50
10	Reference Oosterdijk	4.742, 52.673	3	0-30

The samples were taken largely in accordance with the PFAS sampling guide from the PFAS Expertisecentrum (Expertisecentrum, 2020) and followed the protocol described in Gerardu et al. (2023) to which is referred for detail. In short, samples of 20g for PFAS analysis were taken from the drilled soil material with a pre-cleaned apple corer and stored in 50 mL PE jars pre-rinsed with methanol as to avoid PFAS contamination. Soil for determination of bulk parameters was collected in 250 mL jars. A detailed list of material taken onto the field is found in Appendix A. After being collected, the samples were stored in a 5°C fridge.

Ashes from three Dutch incinerators available at TNO were sampled from bigger bottles and sieved (2 mm) to avoid large chunks for the PFAS analysis. Two samples, labelled BA1 and BA2, are washed bottom ashes (processed) collected in 2016 and 2004, respectively. Another sample is untreated bottom ash from 2014 labelled BA3.

2.3 Soil physical and chemical analysis

The samples were analysed in the TNO laboratory for PFOS, PFOA and a series of other PFAS substances. Soil properties, such as organic matter and organic carbon content, silt and clay fractions, iron and aluminium oxides content, water content and soil pH were measured at the UU Geolab. The latter information is needed to relate the concentration-depth profile to sorption properties of the soil.

2.3.1 PFAS

The samples were analysed for 10 different PFAS substances, which are displayed in Table 2. These substances are among the most found PFAS in Dutch soils (RIVM, 2020).

Table 2. PFAS substances analysed.

PFOS	perfluorooctane sulfonic acid
PFOA	perfluorooctanoic acid
PFBA	perfluorobutanoic acid
PFHpA	perfluoroheptanoic acid
PFNA	perfluorononanoic acid
PFHxA	perfluorohexanoic acid
PFDA	perfluorodecanoic acid
PFBS	perfluorobutane sulfonic acid
PFPeA	perfluoropentanoic acid
PFUnA	perfluoroundecanoic acid

The PFAS pre-treatment and analysis protocol from TNO was followed (available on request) and is described in Gerardu et al. (2023) to which is referred for detail. In short, the samples were first freeze-dried as short-chain PFAS substances such as PFBA, PFBS, PFPeA, PFHxA, PFHpA can be volatile. 0.5 g of freeze-dried soil was used to do the first extraction steps to isolate the PFAS components, using two different solvents. A solid-phase extraction was then performed to concentrate and purify the sample. It was then rinsed with an eluent (1% ammonia in methanol) to collect the PFAS from the stationary phase and then sent to LC-MS analysis to quantify the concentration of each substance.

2.3.2 Organic matter

The bulk soil samples were first freeze-dried and grinded. Organic matter (OM) content was determined by thermogravimetric analysis (TGA) on continuous scanning mode, which consists of repeatedly weighing the samples while they are being increasingly heated from 25ºC (room temperature) to 1000ºC. The organic matter content is the fraction of mass lost between 105ºC and 550ºC, as this is the typical temperature range at which all organic matter gets oxidised. According to Roskam et al. (2008), the mass loss occurring within the range of 450-550ºC results from the oxidation of recalcitrant organic matter, as well as oxidation of ferrous carbonate and dehydration of clay minerals. Between 600ºC and 800 ºC, the mass loss can be primarily attributed to the decomposition of calcium carbonate, and to a lesser extent, to the dehydration of montmorillonite and oxidation of pyrite (Roskam et al., 2008).

2.3.3 Organic carbon

Organic carbon (OC) content was measured using Carbon/Sulfur (CS) elemental analysis. The samples were heated in an induction furnace until their complete combustion and the gaseous products (i.e., CO_2 for organic carbon) were sent to the analyser to detect the carbon elements. The CS elemental analysis was done on two series: one for total carbon (TC) content and one for total inorganic carbon (TIC) content (which consists of all the carbonate minerals) after removal of the organic carbon by hydrogen peroxide treatment. Total organic carbon (TOC) was then calculated by subtracting TIC from TC.

2.3.4 Water content

To determine the moisture content, 2 g of soil samples were weighed and put in a 105°C oven for 48 hours. The samples were then weighed again to obtain dry soil weight and water content.

2.3.5 Grain size

To determine grain size, the Malvern Mastersizer was used for both treated and untreated samples. The pump was set at 2000 rpm and the stir at 750 rpm. Untreated samples were directly injected into the compartment of demineralized water in the Malvern Mastersizer and underwent 60 seconds of ultrasonic shaking until the obscuration reached about 22%. Treated samples were first mixed with 6% hydrogen peroxide to remove all organic matter from the soil. 1N HCl was then added to remove the calcium carbonates. Samples were then ready to be measured in the Malvern Mastersizer and could be classified according to the USDA textural soil classification (USDA, 1987). Grain size was divided into sand (<150 µm), silt (<63 µm) and clay (<8 µm) fractions.

2.3.6 pH

pH was determined according to the Soil Analysis Procedures from Houba (1997). A 1:5 suspension of (wet) soil and demineralized water was prepared and shaken mechanically. The pH was then measured using a pH meter.

2.3.7 Fe and Al oxides

Iron and aluminium oxides were extracted with ammonium oxalate/oxalic acid according to the ISO 12782-3 protocol, as the oxalate extracts the reactive Fe and Al oxides from the sample. Extracts were then measured via inductively coupled plasma (ICP) spectroscopy.

2.3.8 Sorption coefficient K_d

Soil sorption is an important mechanism which affects PFAS mobility and therefore their distribution in the soil column. For instance, long-chain PFAS have a higher sorption affinity and therefore a low potential mobility (Nguyen et al., 2020). Sorption in mineral and organic phases increases with length of chain (Campos-Pereira, 2018). As a result, PFOA is expected to show a higher mobility than PFOS and may, therefore, infiltrate faster in the soil compared to PFOS (Fabregat-Palau et al., 2021). Sorption increases with increasing organic carbon content of the soil and decreases with increasing grain size, as smaller particles have larger surface areas onto which PFAS can adsorb. Lower pH in soils also increases sorption capacity, in particular sorption to ferrihydrites (Campos-Pereira, 2020; Lu et al., 2016). Iron, aluminium and titanium oxides contribute to increased sorption as they offer more mineral binding sites. However, it is of minor importance in soils with organic carbon >2% where organic carbon content, as well as silt and clay fractions, are the primary drivers of PFAS sorption (Fabregat-Palau et al., 2021). Therefore, metal oxides are relevant only when mineral soils are very low in organic carbon (<2%) or when pH is low (Campos-Pereira et al., 2022). Sorption is thus strongly dependent on PFAS type and soil properties (Nguyen et al., 2020).

The sorption coefficient K_d (l/kg) describes the amount of PFAS adsorbed onto the soil in equilibrium with the aqueous concentration. There are different models to predict the K_d value and therefore the potential mobility of PFAS in soils. In this report, three approaches were considered to calculate K_d and use them as input in the transport model of Hydrus.

The first method was developed by Hamaker and Thompson (1972) and is based solely on organic carbon content.

$$K_d = K_{oc} * f_{oc}$$

where K_{oc} is the normalized organic carbon to water partition coefficient and f_{oc} the (measured) fraction of organic carbon in the soil.

K_{oc} was derived from literature, where many different estimates have been deciphered. This report will consider low, mid and high K_{oc} values based on averages retrieved from Nguyen et al. (2020) from different PFAS substances and soil pH. Table 3 shows the different K_{oc} values considered in this report.

Table 3. K_{oc} values chosen from Nguyen et al. (2020).

	low Koc	mid Koc	high Koc
PFOA	1.8	2.3	2.8
PFOS	2.7	3.1	3.5

The second method uses the formula developed by Fabregat-Palau et al. (2021) and is based on organic carbon content, number of CF_2 bonds, and silt and clay fractions.

$$K_d = 10^{(0.41 * \#CF2 - 0.70)} * f_{oc} + 10^{(0.32 * \#CF2 - 1.70)} * f_{s+c}$$

where $\#CF_2$ is the number of CF_2 bonds (7 for PFOA, 8 for PFOS) and f_{s+c} is the measured fraction of silt and clay.

The third method was developed by Wang et al. (2021) to characterize PFOS sorption for a large number of soils and adds the contribution of metal oxide content and silt and clay fractions to the K_d model from Hamaker and Thompson (1972).

$$K_d = f_{oc} * k_{oc} + f_{mo} * k_{mo} + f_{s+c} * k_{s+c}$$

where f_{mo} is the metal oxide fraction, k_{mo} the metal oxide normalized sorption coefficient and k_{s+c} the silt+clay normalized sorption.

Low, mid, and high K_{oc} were retrieved from Table 3 and distribution coefficients k_{s+c} and k_{mo} were established at 19, respectively 7 cm^3/g for PFOS from Wang et al. (2021).

2.4 Transport modelling on Hydrus

The modelling was performed using the Hydrus-1D unsaturated flow and reactive transport model software (version 4.17; Simunek et al., 2008) to calculate content-depth profiles and evaluate the infiltration and accumulation of PFAS in the vadose zone. The model used was based on the tutorial for standard solute transport in multi-layered soil profile (Rassam et al., 2018). The model setup involves 14 pre-processing steps to describe the soil column and its properties, hydraulic parameters, boundary conditions and solute transport parameters.

The model was parametrized using soil physical and chemical data from the two locations (*Scheermer* and *Schapenwei*) for which a high-resolution concentration-depth profile was available, in order to assess the performance of the model and compare the reconstructed PFAS content-depth profiles with the field results. Three different scenarios were tested by varying PFAS deposition in time. In scenario 1, the deposition occurs at a constant rate over the operating years from both the old and the new waste incinerators in Alkmaar, i.e., continuously from 1974 to 2021. In scenario 2, the PFAS emissions are assumed to stop after the shutdown of the old incineration plant in 1996 and there is no deposition at all afterwards. In scenario 3, the deposition is simulated to stop in 2010, when the first PFAS regulations emerged and that current best practice in waste incinerators was then assumed to be sufficient to ensure complete combustion of PFAS, hence deposition is considered null after 2010. The model output that best fits the observed profile will be used to discuss which scenario is most likely to explain whether the PFAS content observed in the soil can be linked to the present and historical emissions from waste incinerators.

It was assumed that no PFAS is leached out of the soil and therefore the total amount of PFAS deposited by the waste incinerator is accumulated in the sampled soil. To determine the total content in the soil, we divided the soil in 10 cm layers and used the following formula to calculate the content per layer C_{tot} in µg/m^2:

$$C_{tot} = L * C * \rho$$

where L is the layer thickness (m), C the content of PFOS or PFOA in µg/kg dry soil (measured) and ρ the bulk density in kg/m^3 according to the USDA soil texture of each layer based on Zeri et al. (2018).

The contents per layer were summed to give the total PFOS/PFOA content per square meter deposited on the soil. It was assumed that the PFAS emissions were constant over the years of operation of the waste incinerator. Therefore, the total content was divided by the total amount of precipitation to determine the concentration of PFAS in the rain in ng/m^3. Meteorological data was retrieved from KNMI for precipitation and reference crop evaporation in the meteorological station De Kooy, which is located about 35 km away from our sampling sites.

For the model setup, we used Standard Solute Transport simulation with Water Flow. We set the number of layers to 8, the depth of the soil profile to 80 cm and the modelling time to 48 years, which corresponds to the years of operation of the waste incineration plant in Alkmaar from 1974 to 2021. The Van Genuchten-Mualem model with air-entry value of -2 cm was selected as it is more suitable for soils with fine textured material such as clay and loam (Rassam et al., 2018). A soil type (based on

USDA soil texture) was attributed to each layer to determine K_s. The upper boundary condition was set as “Atmospheric BC with Surface Layer” and the lower boundary condition as “Constant Water Content”. The sorption constant K_d was calculated for every layer based on the equations in chapter 2.3.8 and put into the Hydrus model for each solute (i.e., PFOS and PFOA). The precipitation, evaporation and solute concentration in the rain were specified in Time Variable Boundary Conditions. In the Graphical Editor of the Soil Profile, we manually divided the soil profile into 8 sub-regions of 10 cm. Other parameters were left as default and details of the model setup are found in Appendix B.

The model was then run and the output files saved. The concentration-depth profile was converted to adsorbed content-depth profile using the following formula.

$$C_{ads}\ (\mu g/kg) = C * K_d$$

where C is the concentration given by Hydrus (µg/l) and K_d is the sorption coefficient (L/kg).

The extracted concentration was given by

$$C_{extr} = C * W_c$$

where W_c is the water content per kg dry soil (kg/kg).

To get the amount expressed per kg dry soil, the adsorbed content was added to the extracted concentration

$$C_{tot}\ (\mu g/kg) = C_{ads} + C_{extr}$$

The model values were plotted as depth profiles together with PFOS/PFOA soil profiles from the field.

3 Results

3.1 Bulk soil analysis

A detailed table with soil physical and chemical results for each depth at every location is found in Appendix C.

3.1.1 Organic matter and organic carbon

Organic matter (OM) accounts for 2 to 23 % of the total sample composition. Total organic carbon (TOC) represents about 40 to 60 % of the OM measured, the rest of the OM consisting of hydrogen, sulphur, oxygen and phosphorus compounds. OM and TOC contents are highest at the surface layer and decrease with depth, except in location 2 and location 9 which show a sudden rise of OM and TOC content at the bottom layer.

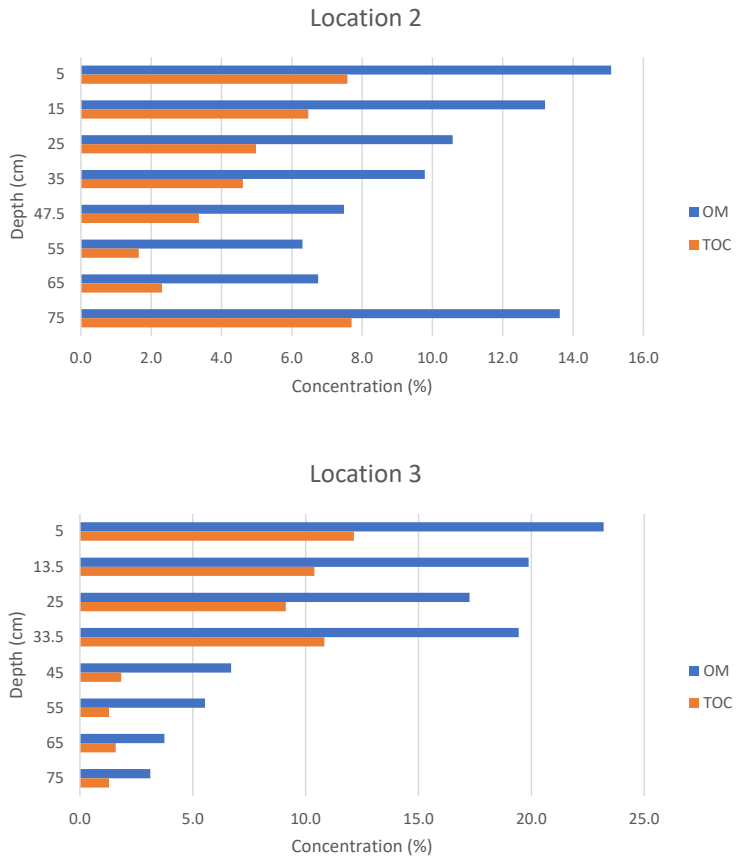

Fig. 4. TOC and OM content at Location 2 and Location 3.

Figure 4 displays the OM and TOC profiles of Locations 2 and 3 (*Schermeer* and *Schapenwei*). OM represents 15%, respectively 23%, of the soil composition at the surface layer for locations 2 and 3. The minimum OM value is reached at 55 cm-bs for Location 2 with 6% OM and 75 cm-bs for Location 3 with 3% OM. TOC ranges from 8 to 12% at the top layer to 1 to 2% at the bottom layer. Detailed TOC and OM profiles for all locations are found in appendix D.

Plotting TOC against OM shows a constant relationship between TOC and OM (Figure 5). The dataset does not exhibit significant deviations. However, four outliers can be observed in the lower left section of the graph, which belong to Location 2 (50-70 cm-bs) and Location 3 (40-60 cm-bs). The slope of the linear trendline is 0.557, which can be used to calculate the conversion factor f_{oc} from OM content, with the relationship f_{oc} = slope * OM.

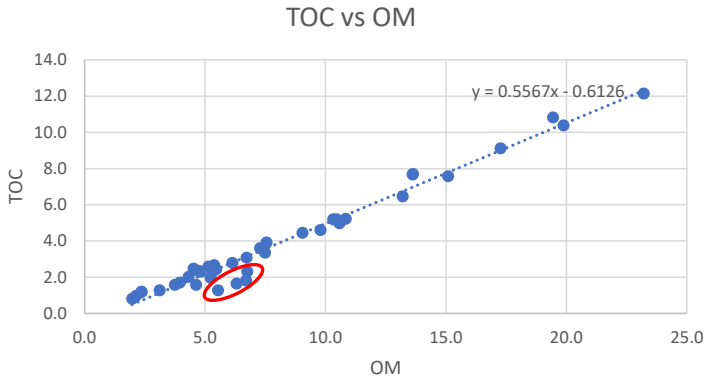

Fig. 5. TOC vs OM graph with linear trendline and its equation. 4 outliers in the red circle.

3.1.2 Grain size

Grain size measurements show that 43% of the soil samples consist of loam, 19% of sandy loam, 14% of silt loam, 11% of clay loam, 5% of silty clay loam, 5% of loamy fine sand and 3% of fine sand. Grain size is very location-dependent, as shown on the USDA soil texture triangle below (Figure 6).

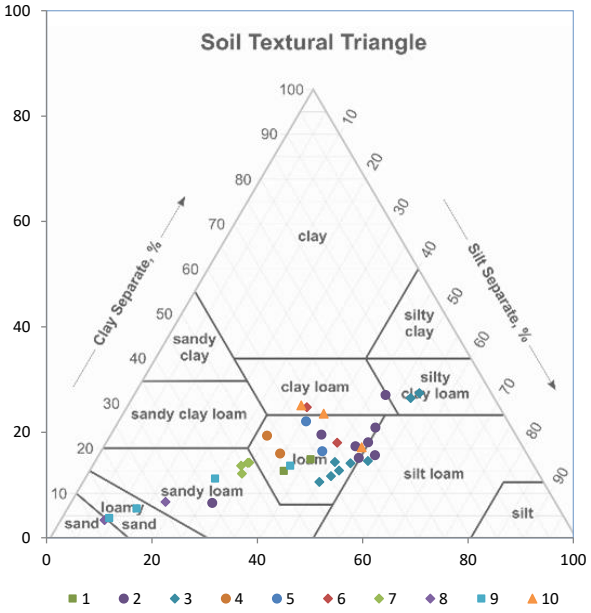

Fig. 6. USDA soil texture triangle by location.

Location 2 has a silt loam texture up to 40 cm-bs and then switches between loam, clay loam and sandy loam as silt content steadily decreases with depth, and sand becomes predominant below 70 cm-bs. Location 3 has a slightly higher grain size

and is composed of loam for the first 40 cm-bs, after which the soil turns into silty clay loam with clay content reaching up to 34% of the total soil composition until 70 cm-bs. The bottom layer displays a loam texture, characterized by a decrease in clay and an increase in sand content. Among all locations in this study, location 8 and reference location 9 show a sandier texture with high sand content throughout their soil profile.

3.1.3 Iron and aluminium oxides

Iron oxide content ranges between 32 and 759 ppm Fe as Fe-oxide and aluminium oxide content between 6 and 72 ppm Al as Al-oxide. In all locations where only shallow samples were collected (i.e., all except *Schermeer* and *Schapenwei*), Fe oxide and Al oxide contents remain below 300 ppm, respectively 30 ppm. Additionally, they remain rather constant throughout the soil profile (Figure 7).

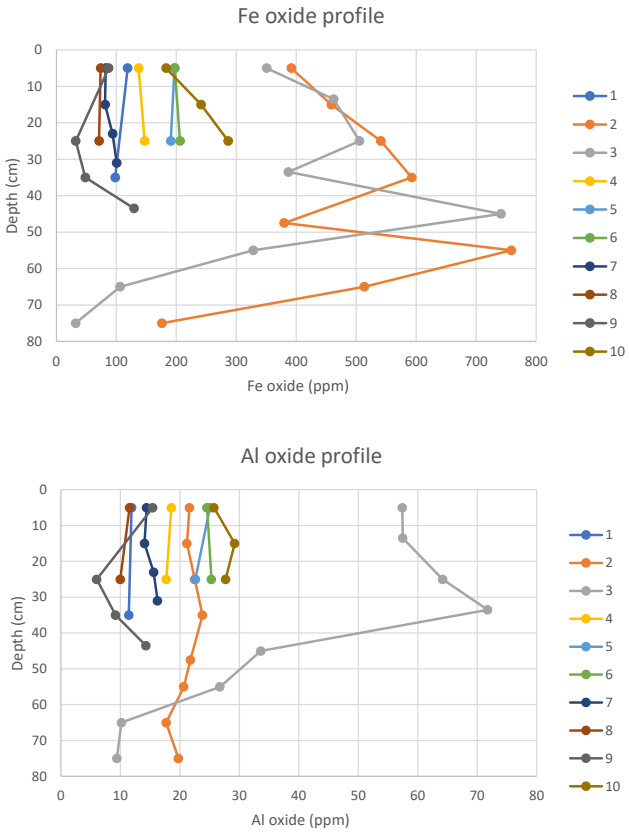

Fig. 7. Depth profiles of Fe and Al oxide contents as based on the oxalate extraction.

Locations 2 and 3 show large variations in Fe oxides and have an overall higher Fe oxide content than the other locations. Between 40 and 60 cm depth, Fe oxide content oscillates strongly between 350 and 750 ppm. The maximum value is reached within this depth interval which is then followed by a rapid decrease in Fe oxide in both locations. In reference location 9, the Fe oxide content initially decreases before subsequently increasing below 30 cm-bs. On the other hand, Fe oxide shows a consistent increase with depth in reference location 10.

At the top, the Al oxide is more than twofold higher at location 3 than the rest of the locations. The Al oxide content peaks at 35 cm depth with 72 ppm, after which it quickly drops to 10 ppm. The behaviour of Al oxide in reference location 9 mirrors that of Fe oxide, with a similar pattern of initial decrease followed by an increase below 30 cm-bs.

3.1.4 pH and water content

The pH value of all samples ranges from 6 to 8 and remains rather constant throughout the soil profiles.

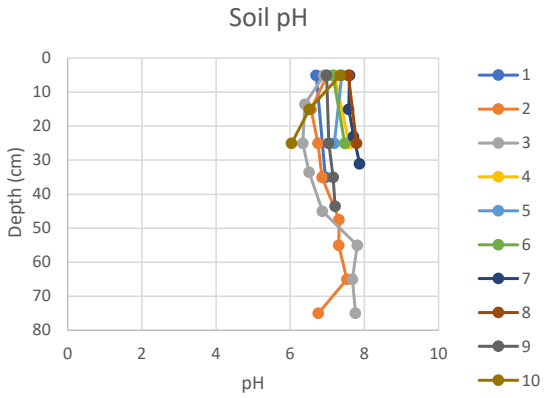

Fig. 8. Depth profile of pH in all locations.

The water content of the samples ranges from 9 to 57 % of the total bulk soil composition. Water content shows a declining trend until a depth of 30 cm-bs. Beyond this depth, the water content starts to increase again consistently across all samples.

Fig. 9. Depth profile of water content in all locations.

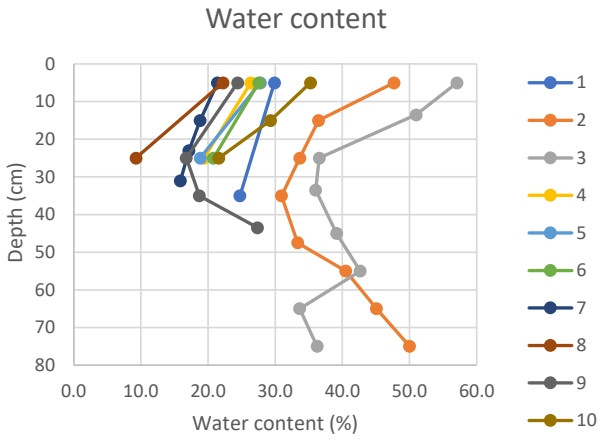

3.1.5 Sorption coefficient K_d

K_d values were calculated for all samples based on the formulas from Hamaker and Thompson (1972), Fabregat-Palau et al. (2021) and Wang et al. (2021). In the formula from Wang et al. (2021), f_{mo} and k_{mo} were not accounted for as pH is higher than 5.0 for all samples. Table 4 shows the different K_d values retrieved for PFOA and PFOS at Locations 2 and 3.

Table 4. K_d values for PFOA and PFOS at Locations 2 and 3.

Location 2, Kd values for PFOA

Depth	Hamaker			Fabregat	Wang		
[cm]	kd low	kd mid	kd high	kd	kd low	kd mid	kd high
0-10	4.79	15.13	47.86	13.69	18.31	28.65	61.38
10-20	4.08	12.91	40.83	11.92	16.96	25.79	53.71
20-30	3.14	9.93	31.41	9.83	16.67	23.46	44.94
30-40	2.91	9.19	29.06	9.38	17.00	23.28	43.15
40-50	2.12	6.69	21.17	7.33	15.11	19.69	34.16
50-60	1.04	3.29	10.40	5.20	16.17	18.41	25.52
60-70	1.46	4.61	14.56	5.60	13.46	16.61	26.57
70-80	4.86	15.37	48.59	12.61	11.54	22.05	55.27

Location 2, Kd values for PFOS

Depth	Hamaker			Fabregat	Wang		
[cm]	kd low	kd mid	kd high	kd	kd low	kd mid	kd high
0-10	38.01	95.49	239.85	33.99	51.53	109.01	253.37
10-20	32.43	81.46	204.62	29.51	45.31	94.34	217.50
20-30	24.95	62.67	157.41	24.08	38.48	76.20	170.94
30-40	23.09	57.99	145.66	22.88	37.17	72.08	159.75
40-50	16.82	42.24	106.10	17.71	29.81	55.23	119.09
50-60	8.26	20.75	52.12	12.03	23.39	35.87	67.24
60-70	11.57	29.06	73.00	13.35	23.57	41.06	85.00
70-80	38.60	96.95	243.53	31.83	45.28	103.63	250.21

Location 3, Kd values for PFOA

Depth	Hamaker			Fabregat	Wang		
[cm]	kd low	kd mid	kd high	kd	kd low	kd mid	kd high
0-10	7.66	24.22	76.60	19.96	18.63	35.19	87.57
10-20	6.55	20.72	65.52	17.46	18.06	32.22	77.03
20-30	5.75	18.19	57.52	15.76	18.22	30.66	69.99
30-40	6.83	21.59	68.28	18.19	18.77	33.53	80.22
40-50	1.15	3.64	11.51	5.69	17.53	20.02	27.89
50-60	0.81	2.57	8.12	4.82	16.78	18.53	24.08
60-70	1.00	3.15	9.97	4.51	12.91	15.07	21.89
70-80	0.81	2.55	8.07	4.29	13.95	15.70	21.22

Location 3, Kd values for PFOS

Depth	Hamaker			Fabregat	Wang		
[cm]	kd low	kd mid	kd high	kd	kd low	kd mid	kd high
0-10	60.85	152.84	383.91	50.34	71.82	163.81	394.88
10-20	52.04	130.73	328.38	43.87	63.55	142.24	339.88
20-30	45.69	114.77	288.29	39.41	58.16	127.24	300.76
30-40	54.24	136.24	342.22	45.70	66.18	148.18	354.16
40-50	9.14	22.97	57.70	13.18	25.52	39.35	74.08
50-60	6.45	16.20	40.70	10.98	22.41	32.17	56.66
60-70	7.92	19.90	49.99	10.55	19.83	31.81	61.90
70-80	6.41	16.11	40.46	9.88	19.56	29.25	53.60

As a result of the higher sorption capacity of PFOS, the K_d values for PFOA are 2.5 to 8 times lower than those for PFOS (using a similar formula). Each calculation method also yields significantly different K_d results. For instance, at the top layer of location 2, the lowest K_d value is 4.79 for PFOA (respectively 38.01 for PFOS) according to Hamaker and Thompson (1972) with low K_{oc}. In contrast, at this specific location and depth, the highest K_d value is 61.38 for PFOA (respectively 253.37 for

PFOS) from Wang et al. (2021) with high K_{oc}. This represents a K_d value increase by a factor of 13 for PFOA (respectively 7 for PFOS) solely based on the K_{oc} and calculation method used. Location 3 shows a high soil sorption at the top layer (e.g., a K_d of 394.88 for PFOS as per Wang et al. (2021) with mid-K_{oc} at 0-10 cm-bs), which then strongly decreases with depth (e.g., K_d drops to 6.41 for PFOS at a depth of 70-80 cm-bs using the previously mentioned method). At location 2, K_d consistently decreases until 50-60 cm-bs. Beyond this depth, it starts increasing again to values similar to the surface layer sorption capacity.

3.2 PFAS analysis

PFAS analyses reveal a significant amount of PFOA and PFOS in most locations, with 21 % and 26 % of the samples showing an elevated PFOA, respectively PFOS content above the background values determined by RIVM (2020).

Soil profiles for both PFOA and PFOS have an enriched top layer, especially in downwind locations. Most profiles follow a bell-shaped pattern, with the maximum PFAS content reached between 10 and 30 cm depth and not directly at the surface. Reference locations show lower total PFOA and PFOS content than downwind locations (Figure 10).

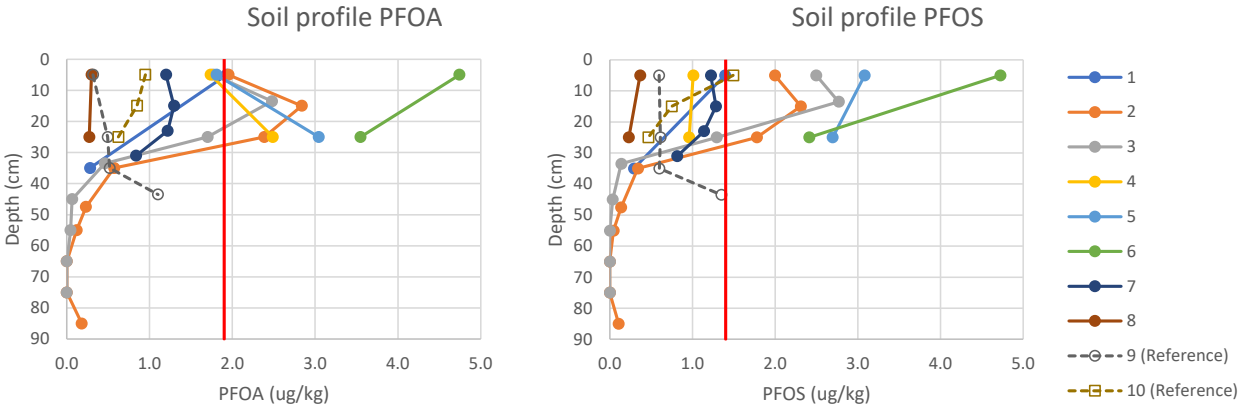

Fig. 10. Depth profiles of PFOA and PFOS compared to RIVM background value (red line).

The highest PFOA and PFOS contents were recorded at location 6 at the top layer, with a value of 4.7 µg/kg dry soil for both PFOA and PFOS. In the top 30-cm layer, 5 locations show higher PFOA (respectively 4 locations for PFOS) content than the background value set by RIVM. Locations 2 and 3 with high profile resolution indicate that the majority of PFAS remain in the top layer of the soil, as PFOA and PFOS content significantly decreases beyond 30 cm-bs, eventually reaching undetectable levels towards the bottom layers. However, location 9 is the only profile in which the trend is reverse and PFAS content increases between 30 and 50 cm depth.

Up to 11 different PFAS species were detected in total. The number of PFAS detected decreases with depth (Figure 11). Most species of PFAS are found in the top layer (<30 cm). Below 50 cm, only PFOA and PFOS are detected in the samples. Downwind locations also contain a higher number of species of PFAS in the topsoil than upwind locations. A detailed table of the species measured in each sample is found in Appendix E.

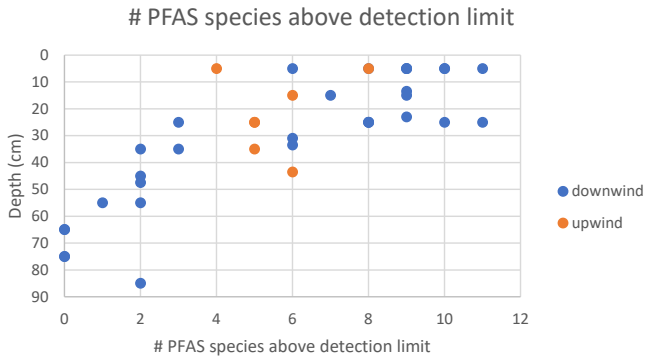

Fig. 11. Number of PFAS species above detection limit vs depth.

The relationship between the cumulative PFAS content present in the top layer and the distance to the waste incinerator in Alkmaar is shown in Figure 12. The PFAS content measured in all depth intervals from 0 to 30 cm-bs were summed together to provide an estimation of the cumulative PFAS content of the top layer for each location. Figure 12 shows that the cumulative PFOA and PFOS content can be up to 6 times higher in downwind location than in reference locations. The PFOA and PFOS content also slightly decreases with increasing distance to the waste incinerator, as indicated by the linear trend. However, the relationship is not very strong (R^2 = 0.14 for PFOA, resp. 0.16 for PFOS). It is also important to note that locations 7 and 8 (in red circle) have likely experienced some form of disturbance over the past 50 years and should therefore be carefully considered when interpreting the data. The grey dashed line is an illustration of the overall trend that is observed for the PFOA/PFOS content as it varies along the distance. Initially, the PFOA and PFOS contents increase until they reach their highest peak approximately 700 m away from the waste incinerator (Location 6). Farther away, the PFOA and PFOS contents gradually decrease as the distance from the incinerator increases.

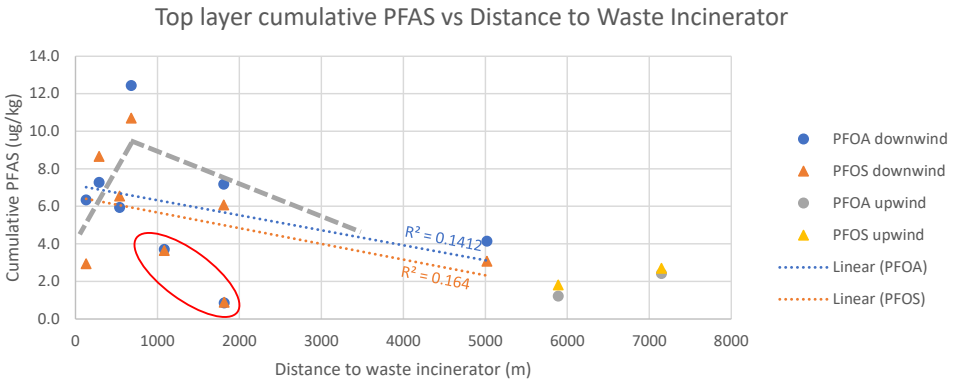

Fig. 12. Top layer cumulative PFAS vs distance Alkmaar waste incinerator. The red circle indicates the likely disturbed locations and the grey dashed line is an illustration of the overall trend of the PFOA/PFOS content along the distance.

Figure 13 below displays the correlation between PFOA and PFOS. The best-fit linear regression for downwind locations has a slope of 0.884, indicating that the PFOA:PFOS relationship follows a consistent ratio of approximately 1:0.88. Additionally, the PFOA:PFOS ratios obtained from ashes and reference locations align closely with the trend derived from downwind locations.

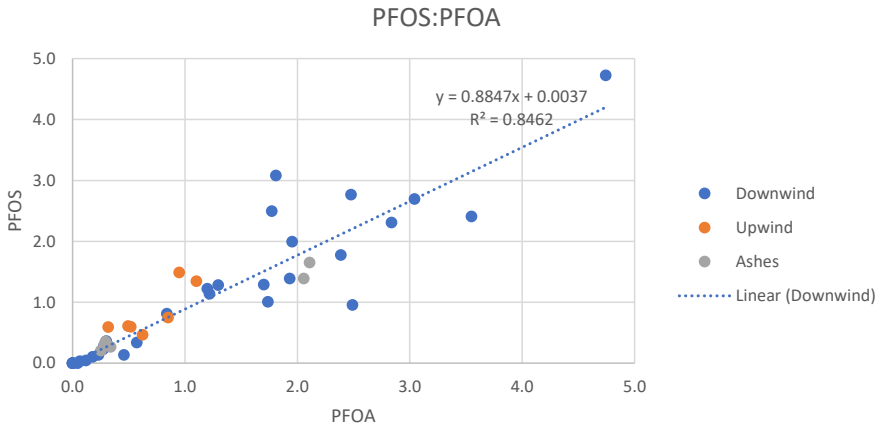

Fig. 13. PFOS vs PFOA relationship.

The BA1 and BA2 ashes exhibit notably low levels of PFOA and PFOS content, falling well below the background values provided by RIVM. In contrast, BA3 can be considered as contaminated since it surpasses the background limits for PFOA and PFOS, with content values of 2.1 µg/kg and 1.5 µg/kg respectively. However, it is worth noting that BA3 was the only untreated ash sample analysed, as both BA1 and BA2 had been processed and washed at the waste incinerator prior to analysis. BA1 and BA3 follow a PFOS:PFOA ratio consistent with the trend depicted in Figure 14, as PFOA content is slightly higher than PFOS. PFOA and PFOS also closely follow each other in terms of content levels as they are both elevated (BA3) or relatively low (BA1 and BA2).

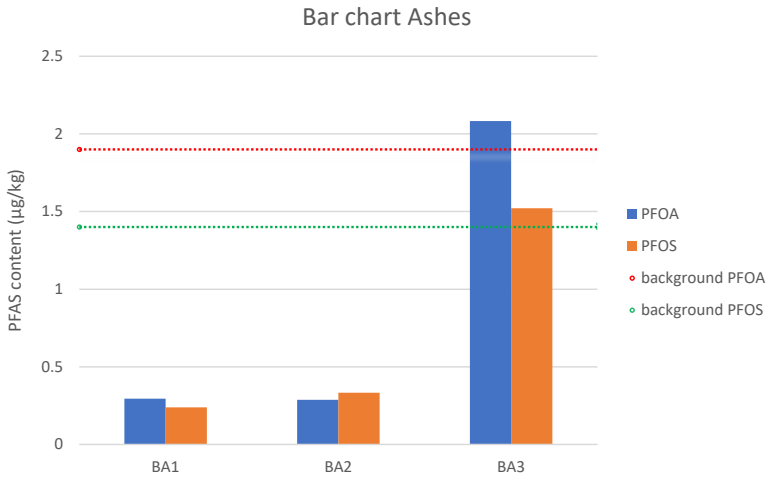

Fig. 14. PFOA and PFOS content in three bottom ashes.

3.3 HYDRUS results

The soil profiles generated by Hydrus along with the field measurements are presented on pages 27-30 (Figures 15-18). The different scenarios described as “low Ham”, “mid Ham” or “high Ham” correspond to model outcomes with K_d calculated according to Hamaker and Thompson (1972) with either low, mid, or high K_{oc}. “Fabr” refers to the method developed by Fabregat-Palau et al. (2021) to determine K_d. Similarly, the terms “low Wang”, “mid Wang” and “high Wang” stand for K_d scenarios based on Wang et al. (2021) with low, mid and high K_{oc}.

Different K_d inputs in the model generate very different peak shapes, transport behaviour and PFAS content in the soil. High K_{oc} values result in large peaks in the first 10 cm-bs (see high Ham and high Wang curves on Figures 15-18) and large decreases beyond that depth, with no PFAS reaching depths below 40 cm-bs. The 1996 and 2010 scenarios generally produce a bell-shaped pattern with the highest peak below the soil surface at a shallow depth (0-10 cm-bs for PFOS, 0-30 cm-bs for PFOA). The constant emission scenario shows highest PFOA and PFOS values right at the surface with a large decline in PFAS afterwards. The constant emission scenario thus did not match well with the field measurements, as field observations revealed a significant peak at 10-20 cm-bs which was not captured in the constant emission model.

For PFOA, high Ham and high Wang models have very similar shapes, although the peak from high Wang shows a slightly higher content in PFOA than from high Ham. The curves from Fabregat and mid Ham are also very similar to each other and follow the same trend, with a PFOA concentration distributed over the first 50 cm depth and peaking at either 20 cm-bs (2010 scenario) or 40 cm-bs (1996 scenario). With the Hamaker method and low K_{oc}, PFAS were washed away right after deposition and almost no PFAS was adsorbed by the soil until a higher depth (from 70 cm-bs). Among the different scenarios considered, the mid-Wang curve from the 1996 scenario exhibits the closest match to both the intensity of the content peak and the overall profile curve observed from the field measurements.

The results of the Hydrus model also show a large disparity in the adsorption effects between PFOA and PFOS, with PFOS exhibiting considerably higher adsorption in the top layer than PFOA. The capacity of the surface layer to retain PFOS can be up to twice as much as that of the modelled PFOA, although field observations have demonstrated a similar soil profile curve for both PFOA and PFOS. High Wang and high Ham for PFOS generate a comparable shape to that of PFOA, but their peak content is 4 to 10 times higher than the PFOS field measurements. Mid Wang and mid Ham show a similar trend, but their highest peak reaches only about half the intensity of the ones from high Wang and high Ham. The curves from low Ham and Fabregat in the 1996 scenario provide the best fit to the observed data in terms of peak intensity and general shape of the content profile, although their peaks remain 5-10 cm shallower than the field measurements.

Location 2 - PFOA

Fig. 15. Modelled vs observed depth content profiles of PFOA for Location 2.

Location 2 – PFOS

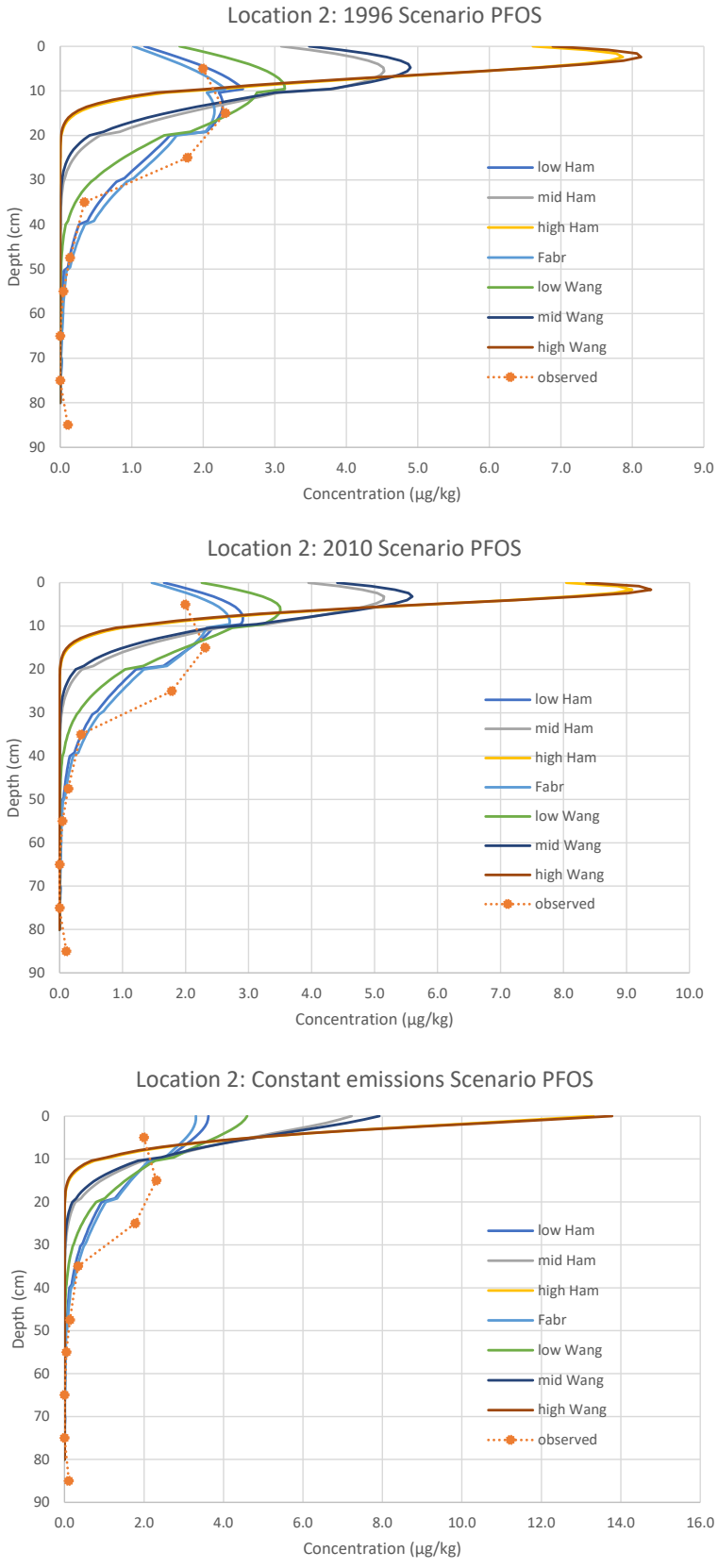

Fig. 16. Modelled vs observed depth content profiles of PFOS for Location 2.

Location 3 – PFOA

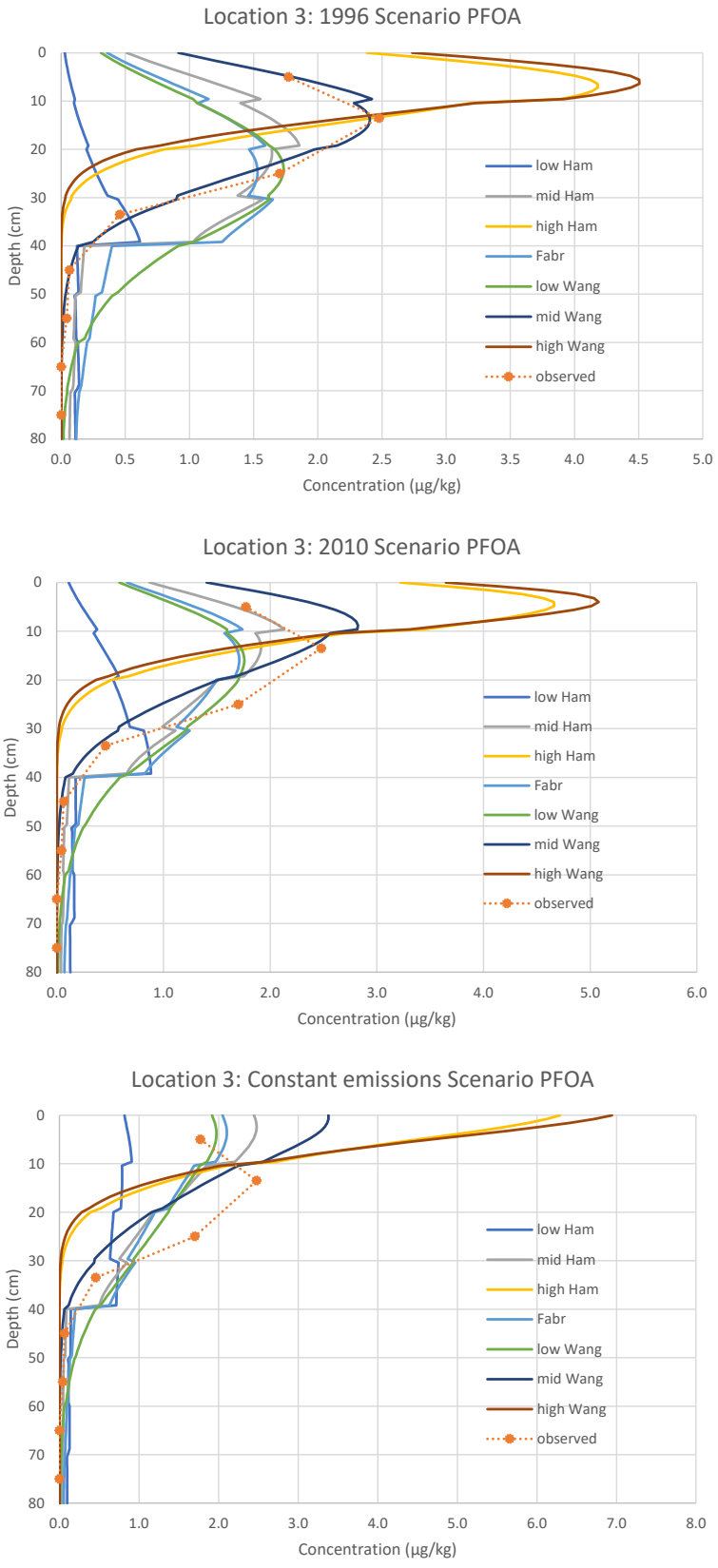

Fig. 17. Modelled vs observed depth content profiles of PFOA for Location 3.

Location 3 – PFOS

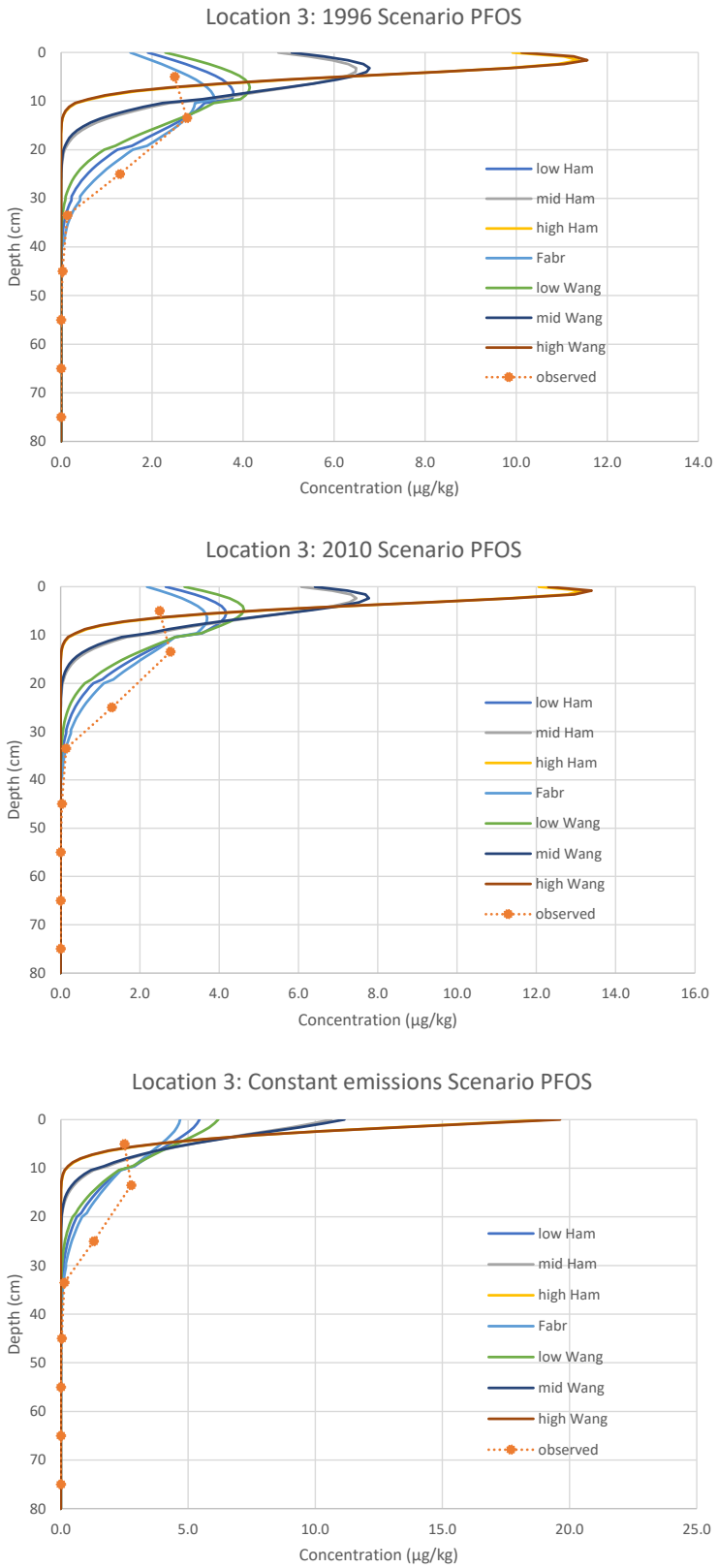

Fig. 18. Modelled vs observed depth content profiles of PFOS for Location 3.

4 Discussion

This chapter discusses the bulk soil analysis, in particular the TOC and Fe and Al oxides, followed by the findings of the PFAS analyses and the HYDRUS model.

4.1 Bulk soil analysis

TOC

The observed ratio TOC/OM of 0.557 in the soils is consistent with the rather narrow bandwidth that is found for natural humic substances in a variety of natural and anthropogenic materials (Van Zomeren et al., 2008). The four outliers in the OM vs TOC graph (Figure 5) are unexplained, but may be explained by their high clay and water content compared to most of the other samples, which could play a role in their enrichment in OM relative to TOC. Another potential explanation could be an overestimation of OM by TGA that is not corrected for clay dehydration.

Fe and Al oxides

The rapid alternation of Fe oxide content between the depths of 40 and 60 cm-bs (Figure 7) suggests large fluctuations in groundwater levels. Indeed, iron oxides in clayey soils are highly dependent on hydrology and accumulates above the groundwater table. When the groundwater level rises, iron oxides precipitate. However, with increasing depth, the Fe content decreases due to the prevailing reduced conditions, leading to the dissolution of Fe oxides into Fe^{2+} and resulting in the sediment acquiring a greyish coloration. The significantly lower Fe oxide contents observed in other locations may be attributed to the absence of seepage and the lack of groundwater infiltration from below into these layers.

The elevated Al oxide content observed in location 3 (Figure 7) can potentially be attributed to variations in mineralogy or clay content. Further analysis and characterization of the soil composition in location 3 could provide more insights into the drivers of this high Al oxide content.

4.2 PFAS analysis

The PFAS depth soil profiles (Figure 10) reveal that the highest PFOA and PFAS contents are found between 10 and 20 cm-bs, rather than directly at the surface. As the depth increases, PFOA and PFOS contents gradually decrease. Locations 2 and 3 (*Schermeer* and *Schapenwei*) with high-resolution profiles exhibit a very distinct bell-shaped pattern. Since these two locations were undisturbed for decades and PFAS migrated downwards, this suggests that emissions were higher in the past compared to current emissions, leading to the accumulation of PFAS at deeper layers in the soil over time. This situation is quite similar to the findings regarding PFOA content in the soil profile nearby a fluoropolymer factory in Dordrecht (Gerardu et al., 2023). Hence the observed PFAS content in the soil can be considered an indicator of historical emissions rather than solely reflecting current emissions. The absence of alternative nearby sources also suggests that the old waste incinerator played a

significant role in the PFAS content observed in the soil profile. It is very probable that past combustion processes were less efficient at waste incinerators and resulted in higher levels of atmospheric contamination compared to present times. Old incinerators were likely operating under suboptimal conditions, with insufficiently high temperatures, inadequate oxygen content, and the absence of scrubbers to remove contaminants from the flue gases. However, it remains uncertain if all accumulated PFAS can be attributed to the activity of the old waste incineration plant alone, as the overall amount of waste burned was much lower and may or may not have contained less PFAS compared to now. Past activities in the area such as industrial processes might have also contributed to the soil contamination, although there are no clear indications for other local sources as well.

In addition, both PFOA and PFOS exhibit the same bell-shaped pattern within their respective soil profiles and have their peak front occurring at the same depth (except in locations 4 and 5). This is somewhat unexpected, as the higher soil adsorption capacity of PFOS should result in PFOS being less mobile and more present closer to the surface compared to PFOA. This similar distribution pattern in the soil profile can be explained by several reasons, for example the soil composition affecting the adsorption and retention of PFAS compounds. It is therefore possible that the soil mineralogy, organic matter content, and silt+clay content in this study area strongly mitigate the downward transport of both PFOA and PFOS. Moreover, the complex sorption mechanisms of PFAS are influenced not only by soil properties, but also by the presence of competing substances or even root uptake by plants (Mei et al., 2021), affecting the mobility of PFOS and PFOA and potentially resulting in a more even distribution. Additionally, the air-water interface (AWI) could play a significant role in PFAS sorption, especially at the relatively low PFAS contents found in this study (Gerardu et al., 2023). A less plausible explanation may be that PFOA and PFOS do not share the same sources in this area, and that PFOS thus could have been emitted earlier than PFOA and/or in larger amounts.

Some additional observations can be made regarding the PFAS soil profile (Figure 10). In location 2, a sudden increase in PFOA and PFOS content at a depth of 80-90 cm-bs can be seen based on a single data point, for which no clear explanation has been identified. No sampling was conducted at greater depths which could confirm or deny this observation. Location 4 shows a high PFOA content which increases with depth, whereas on the contrary its PFOS content is low and remains constant throughout the soil profile. This can be due to the fact that this sample was collected directly by the waste incineration plant, next to a ditch and a public road, which may be both sources of PFOA contamination at this specific location. Additionally, these observations rely on a mere two data points. As a result, it is difficult to draw conclusions due to the potential influence of analytical errors (which might extend to tens of percent) attributed to low recovery during the laboratory procedures. Furthermore, location 6 also exhibits notably high PFOA and PFOS contents at the surface. This could be attributed to its proximity to both the old and new incinerators, as well as a nearby road (5 m away). The limited downward transport of PFAS at this location may also be influenced by the soil composition, particularly the presence of 20-28% clay which increases the adsorption and retention of PFAS. Moreover, the elevated PFOA and PFOS content observed may result from recent contamination as PFOS are still concentrated at the surface while PFOA already penetrated into a deeper layer (20-30 cm-bs) due to its higher mobility. Location 5 is located very close to location 6 and similarly shows high PFOA and PFOS contents. However, its PFOA

content increases with depth while the PFOS content shows a slight decrease. This behaviour may indicate that all PFOA was washed away and therefore its peak content is already deeper below the surface, or it may suggest that PFOA and PFOS originate from different contamination sources at this location. The results observed could also potentially arise from analytical uncertainty, as the dataset at this location comprises only two data points. Inversely, PFOA and PFOS content are very low at location 8. This location, 30 m away from a canal, is suspected to have been disturbed recently due to road works, hence the soil collected might not be representative of the study area. Location 7, in close proximity, might have undergone similar disturbances. It is therefore difficult to interpret and draw conclusions from these two locations. Reference location 9 has an atypical soil profile shape, with a sudden increase of PFAS content below 40 cm-bs. Location 9 is situated within a nature conservation area most likely devoid of any other possible, non-atmospheric PFAS sources for the past few decades. The sample was however obtained on the slope of a dyke, which could have been slightly disturbed when PFAS-containing sediment dredged from the canal was deposited against the dyke.

Figure 12, depicting the cumulated PFOA and PFOS content in the soil top layer versus the distance to Alkmaar waste incinerator, indicates a weak correlation between the presence of PFAS compounds in the soil and the proximity to the waste incinerator. The PFOA and PFOS contents in the soil tend to be higher in downwind locations that are closer to the waste incinerator than in the reference locations. The highest PFAS content is found at approximately 700 m away from the waste incineration plant, and then gradually diminishes over the next 5 km. It is coherent that the majority of PFAS deposition occurs a few hundred meters away from the waste incinerator rather than directly adjacent to it, as the particles emitted from the chimney are carried away by the wind before depositing. This is also in accordance with the findings of Mennen et al. (2010) who predicted the highest deposition levels of dioxin, another persistent organic pollutant, to occur within a range of 1-2 km from an industrial plant. However, it is difficult to determine whether the wind direction has a notable influence on the deposition and accumulation of PFAS in the vicinity of the waste incinerator. A comparison between downwind and reference locations is complicated due to the careful selection of undisturbed reference locations, which are thus situated at a considerable distance (>5 km) from the waste incinerator. Finding closer reference locations in the West direction was challenging due to the presence of the city of Alkmaar directly next to the waste incinerator. Besides, there is dominance in wind directions in the Netherlands, however the wind comes from any direction over the course of a year. The omnipresence of PFAS in the Netherlands makes it hard to identify unloaded areas for comparison.

According to a report by SWECO (2019) on PFOA and PFOS levels in North-Holland, there were slightly elevated PFAS levels observed in the NE direction of Alkmaar (0.7 µg/kg for PFOA, 0.5 µg/kg for PFOS respectively), however well below the RIVM background values. The report does not provide sufficient detail and resolution to establish a relationship between the PFAS content measured and the waste incineration activities. Furthermore, it does not offer any indication regarding the potential sources of PFAS in the region. In particular, elevated contents (up to 2.6 µg/kg for PFOA, 1.2 µg/kg for PFOS respectively) near the Markermeer and the IJsselmeer remain unexplained, as these locations are away from any known industrial activities or waste incinerators.

The relationship between PFOA and PFOS is very narrow (Figure 13). PFOA content in soil is consistently slightly higher compared to PFOS content, a pattern that remains consistent throughout the soil profile for a majority of samples and can even be observed in the ashes' composition and the reference locations. This consistent relationship can be attributed to various factors, such as production practices and waste composition which may have remained relatively constant over the past 50 years. Notably, reference locations, which are expected to be undisturbed, also display the same ratio. The relationship between PFOA and PFOS thus holds consistently across different sample types and environmental contexts.

Another interesting observation is that most PFAS compounds are undetectable below a depth of 30 cm-bs, except for PFOA and PFOS, which show higher persistence at deeper layers (Figure 11). This could be explained by the significantly lower concentrations of other PFAS compounds in the soils compared to PFOA/PFOS. The detection limit for all PFAS compounds is equal to 0.3 µg/kg. Consequently, with decreasing concentrations as a function of depth, it is plausible that the other PFAS compounds drop below the detection limit more quickly than PFOA/PFOS. The prevalence of PFOA and PFOS in the soil may also be due to the fact that they were among the first types of PFAS produced on a large scale and broadly used in various consumer products, which explains their widespread presence in soils all around the Netherlands (Buck et al., 2011). The presence of a higher variety of PFAS species in the soil top layer can therefore also result from their relatively recent manufacturing and subsequent release into the surrounding environment. As production processes evolve and continuous development of new PFAS compounds occur, it is possible that alternative PFAS substitutes, such as the fluorinated compound GenX, may become predominant in the upper soil layers in the future (Brandsma et al., 2019).

Ashes

Ash sample BA3 provides evidence that PFOA and PFOS were initially present in the waste prior to the incineration and that not all PFAS compounds are fully degraded during the combustion process. While some PFAS may adhere to the fly ash and bottom ash particles, others may also be volatile at elevated temperatures and escape with other flue gases. Since PFOA and PFOS persist in the ashes after incineration, there is also a probability that they could be present in flue gases and get released into the atmosphere through the incinerator chimney.

Furthermore, the analysis of ash samples demonstrates the effectiveness of washing to remove PFAS, as treated ash samples (BA1 and BA2) show significantly lower levels of both PFOA and PFOS compared to the untreated ash sample BA1. However, while the washing process successfully reduces the presence of PFAS compounds in the ashes, it will also generate waste water which, if not properly treated, may release PFAS into nearby surface waters (Jans & Berbee, 2020).

4.3 HYDRUS modelling

The Hydrus simulations conducted for PFOS transport (Figures 16 and 18) reveal significant disparities between the model predictions and the actual field observations. In contrast to the field observations where the peak content was found at a depth of approximately 15 cm-bs, the simulations consistently showed the

highest content within the first 0-10 cm-bs, follow by a very rapid decline. Additionally, the simulated PFOS peak content was up to four times higher than the measured peak content values obtained from the field. The Hydrus model for PFOS thus inaccurately estimates peak intensities and underestimate the depth at which the peak front is observed. This deviation between field observations and model outcomes is likely the result of an overestimation of the soil adsorption effect in most Hydrus simulations for PFOS. Simulations with low K_d values (low Hamaker, low Wang and Fabr) indeed provided the most accurate estimations of PFOS depth content profiles. This aligns with the Hydrus simulations conducted by Gerardu et al. (2023) which demonstrated that model scenarios based on low K_{oc} values reproduced the PFOS depth content profiles closest to the observed data.

The Hydrus model is very sensitive to K_d variations, as each simulation generated significantly different results. An accurate estimation of K_d is therefore crucial for obtaining reliable results with the model. It is however difficult to determine which method is most appropriate to calculate K_d, as it very depends on the compound and the specific location investigated. Due to the unreliability of the estimations, it is therefore advisable to directly measure K_d for greater accuracy in future modelling efforts.

Soil texture is another factor that has a large influence on the model, as can be observed from Figure 17, where a large decrease in PFOA content can be seen at 40 cm-bs in low Ham, mid Ham and Fabr, or also in Figure 15, where a sudden increase in PFOA content occurs at 70 cm-bs for low Ham, mid Ham and Fabr as well. Although these trends were not observed in the actual data, these abrupt changes in the model results coincide with transitions in soil texture, specifically from loam to silty clay loam and from loam to sandy loam, respectively. Soil texture, in addition with K_d, therefore plays a substantial role in the modelled transport behaviour of PFAS. Additional factors, such as silt+clay content, temperature, pH, water content and organic matter content also significantly affect the sorption and transport behaviour of PFAS. Accurately parametrizing these variables is essential for achieving more refined model outcomes.

Furthermore, the version of the Hydrus model employed in this study did not account for the air-water interface. AWI sorption can be approached as linear sorption process at the low PFAS contents found in this study (Gerardu et al., 2023). Therefore, K_d values deployed in this study may implicitly reflect AWI sorption to some extent, even though these are based on presumed interaction with organic matter and/or clay. However, the incorporation of the air-water interface is still an important consideration for future modelling efforts.

The 1996 and 2010 scenarios for PFOA and PFOS (Figures 15-18) consistently show very similar shapes of soil profile. Both scenarios also generate the closest match to the field values. This provides evidence that the PFAS content observed in the soil profile is indeed a consequence of historical activities rather than current emissions. Specifically, the 1996 scenario, which often aligns more closely with the field observations due to its deeper peak front, suggests that the decline of emissions occurred more than 20 years ago, and that the primary source of PFAS contamination is no longer active. Furthermore, the constant emission model consistently fails to accurately reproduce the field results, indicating that it is not a realistic representation

of the current situation and further supporting the idea that emissions have ceased or diminished considerably over time.

Another interesting observation is that the K_d obtained by the Wang et al. (2021) and Hamaker & Thompson (1972) methods yield very different model outcomes, highlighting the substantial impact of including the silt+clay effect on soil adsorption. Moreover, the study conducted by Wang et al. (2021) was primarily intended to describe transport behaviour and sorption of PFOS and its associated parameters, including K_{s+c}. However, the same K_{s+c} was applied for PFOA to calculate its K_d, and the results obtained match closely the field observations, as mid-Wang provide the best fit to the field data for PFOA (1996 scenario).

Parameters such as sorption coefficient, PFAS compounds, soil texture and other influential factors all contribute significantly to the overall results. More sophisticated PFAS transport models which account for a wider range of factors and not only consider linear sorption as the sole retention process, may capture more accurately the complexity of PFAS transport behaviour in the soil. Furthermore, constant emissions from the waste incinerator throughout its operational years were assumed and do not reflect the changes in waste quantities incinerated over time. Significant changes in the total amount of waste processed have been observed, with a notable increase from 325 kton of waste burned in 1970 in the Netherlands to approximately 8000 kton/year since 2014 (CLO, 2021). This could indicate that there has also been an increase in volume of activity at the Alkmaar waste incinerator over the last five decades. Hence more data on the emission history of the old incineration plant, the volume of waste processed, and its combustion methods are necessary to better assess its influence on the observed PFAS soil profile. Identifying other historical sources of PFAS in the area and investigating potential contribution of unknown sources of PFOA and/or PFOS with the Hydrus model could provide valuable insights and improve the accuracy of the model.

4.4 Other potential sources of PFAS

If the observed PFAS content in the soil profile cannot be solely attributed to the activities of the waste incinerator, it is relevant to consider other potential sources that could have contributed to the contamination.

4.4.1 Sea spray aerosols

Sea spray aerosols (SSA) are droplets of seawater in suspension formed by bubbles bursting on the sea surface. When waves break into the water, air mixes with seawater and creates bubbles, which rise to the surface and burst, releasing droplets of seawater into the air and scavenging PFAS from the air-water interface into the atmosphere (De Leeuw et al., 2011; Sha et al., 2021; Johansson et al., 2019). They can also reside in the atmosphere from seconds (for larger particles) to days (for smaller particles) (De Leeuw et al., 2011). Due to their aqueous surface tension and their moderate hydrophobic character, a large amount of PFAS remain at the sea-surface microlayer (a layer between 1 and 1000 µm at the surface of the ocean), where they can easily be transferred back to land through SSA formation and transport (Casas et al., 2020; Johansson et al., 2019). Recent studies from Sha et al. (2021) and Casas et al. (2020) have shown that SSA are enriched in PFAAs (among

which are PFOA and PFOS) and could therefore be a major source of PFAS contamination in coastal areas, as well as in remote areas such as Antarctica. The PFAS deposition is dependent on the origin of SSA and decreases with increasing distance to open water (Sha et al., 2021). It is therefore possible that PFAS released from rivers (e.g., from England into the North Sea) remain at the air-water interface and pushed with the wind towards the coast of the Netherlands.

This hypothesis is also supported by the report from SWECO (2019) which presents elevated PFOS content on the coast of North-Holland. In addition, Sha et al. (2021) have determined that SSA can travel distances up to 300 km in the atmosphere (for SSA with r_{80} = 5 µm). Alkmaar waste incinerator is located about 10 km from the sea, which suggests that SSA may well be a significant source of PFAS in the area. However, the reference locations (#9 and #10) are situated considerably closer to the sea (respectively 4.6 and 7.5 km; see Figure 3). Contents at these reference locations are below (PFOA) or similar to (PFOS) the RIVM background values while contents downwind the incinerator are predominantly higher (Figure 10), indicating that the contribution of SSA is relatively small. Further research with high-resolution core samples in the undisturbed dune area may help to better understand the contribution of sea spray aerosols to the diffuse PFAS pollution in the region.

4.4.2 Other potential sources

Frequent forest fires in the dunes of North-Holland in recent years could potentially explain the elevated levels of PFOS detected by SWECO (2019) in the dunes near Alkmaar, as PFOS were commonly used in firefighting foam up until 2012 (Ruyle et al., 2023). Further research is needed on the possibility that the use of fire-extinguishing foam during these fires may have contributed to the presence of PFOS (and more generally PFAS) in the affected areas, and therefore also potentially contaminating the soil closer to the waste incineration plant.

5 Conclusions

1. Can the PFAS deposition profile be linked to the historical activity of waste incineration plants?

1.1 Do the ashes of waste incinerators contain PFAS which survived the incineration process?

Analysis of ash samples have revealed that PFAS can apparently survived the incineration process and adsorb onto the bottom ash. This finding suggests that PFAS compounds are not fully degraded during combustion and may also persist in the flue gases, potentially being released into the atmosphere.

1.2 Is there a contrast in the PFAS soil content in the predominant wind direction (SW) from waste incinerators?

The eight locations located downwind of the incinerator exhibited higher levels of PFAS in the soil top layer (<30 cm) when compared to the 2 reference locations. However, it is important to approach these conclusions cautiously given the large distance (>5 km) between the reference locations and the waste incinerator. Furthermore, despite prevailing southwest winds in the Netherlands, the variability of wind direction throughout the year and the widespread presence of PFAS in the Dutch environment complicate direct comparisons.

1.3 Is it possible to find a correlation between PFAS and the distance to the waste incinerator?

A weak correlation was found between the PFAS content in the soil and the distance to the Alkmaar waste incinerator. Additionally, the highest deposition was situated about 700 m away from the waste incineration chimney, rather than directly adjacent to it, and subsequently decreased with increasing distance. This observation supports the hypothesis that PFAS were emitted from the waste incinerator and transported by the wind before deposition. Moreover, a distinct bell-shaped pattern emerged in the high-resolution cores, suggesting that the observed PFAS content-depth profiles are indicative of historical emissions and that the primary source of PFAS contamination has ceased. The waste incinerator was therefore likely a substantial contributor to the observed PFAS content in the past, although the precise extent of its influence remains to be established.

1.4 Can the reactive transport model Hydrus-1D be used to model the transport of PFAS in soil profiles, given the possible PFAS atmospheric deposition from waste incinerators?

The Hydrus model demonstrated its ability to reconstruct PFAS deposition and transport in the soil. The best-fit scenarios, characterized by emissions stopping in 1996, mid-Wang curve for PFOA, respectively low Ham curve for PFOS, align with the hypothesis that past emissions from the waste incinerator may explain the observed PFOA/PFOS content-depth profiles. However, the selection of parameters can significantly influence the outcomes of the model. In particular, determining the

most suitable sorption coefficient K_d for each PFAS compound to accurately replicate their behaviour in the soil remains a challenging task.

2. If not, which other possible diffuse sources may contribute to the observed PFAS concentrations?

Sea spray aerosols or PFAS from firefighting foams used during forest fires in the dunes near Alkmaar may potentially contribute to the diffuse contamination in the area. However, the impact of these factors appears limited, and no significant alternative sources of PFAS have been identified in the region.

In conclusion, this study presents a significantly enhanced resolution of the area located downwind of the Alkmaar waste incinerator. It has provided a more detailed and precise understanding of the spatial distribution, extent, and characteristics of the PFAS diffuse contamination within the area. Getting a deeper insight into the fate and transport of PFOA and PFOS in the soil is essential for forecasting, for instance, the possibility of their leaching into the groundwater.

Recommendations

Expanding the sampling efforts through the collection of additional samples at connected intervals and reaching greater depths would contribute to obtaining an even more complete picture of the PFAS distribution in the area. The historical emissions from the waste incinerator, based on the waste composition, volume of waste processed and operational factors, also need to be carefully assessed to better understand its contribution to the presence of PFAS in the area. In addition, direct sampling of flue gases would provide valuable insights into potential emissions of PFAS into the environment due to ongoing waste incineration practices. Further research is also needed to measure soil-specific sorption coefficients which would substantially improve the accuracy of PFAS sorption modelling.

6 References

3M Company. (1999). *Fluorochemical use, distribution and release overview* (No. AR226-0550). USEPA Administrative Record.

Ahrens, L., Shoeib, M., Harner, T., Lee, S. C., Guo, R., & Reiner, E. J. (2011). Wastewater treatment plant and landfills as sources of polyfluoroalkyl compounds to the atmosphere. *Environmental Science & Technology, 45*(19), 8098-8105.

Aleksandrov, K., Gehrmann, H., Hauser, M., Mätzing, H., Pigeon, D., Stapf, D., & Wexler, M. (2019). Waste incineration of polytetrafluoroethylene (PTFE) to evaluate potential formation of per- and poly-fluorinated alkyl substances (PFAS) in flue gas. *Chemosphere, 226*, 898-906.

Awad, R., Bolinius, D.J., Strandberg, J., Yang, J.-J., Sandberg, J., Bello, M. A., Gobelius, L., Egelrud, L., & Härnwall, E.-L. (2021). *PFAS in waste residuals from Swedish incineration plants. A systematic investigation* (Report No. B 2422). IVL.

Bakker, J., Bokkers, B., & Broekman, M. (2021). *Per- and polyfluorinated substances in waste incinerator flue gases* (Report No. 2021-01143). RIVM.

Boisvert, G., Sonne, C., Rigét, F. F., Dietz, R., & Letcher, R. J. (2019). Bioaccumulation and biomagnification of perfluoroalkyl acids and precursors in East Greenland polar bears and their ringed seal prey. *Environmental Pollution, 252*, 1335-1343.

Brandsma, S. H., Koekkoek, J. C., van Velzen, M. J. M., & de Boer, J. (2019). The PFOA substitute GenX detected in the environment near a fluoropolymer manufacturing plant in the Netherlands. *Chemosphere*, *220*, 493–500.

Buck, R. C., Franklin, J., Berger, U., Conder, J. M., Cousins, I. T., De Voogt, P., . . . Van Leeuwen, S. P. (2011). Perfluoroalkyl and polyfluoroalkyl substances in the environment: Terminology, classification, and origins. *Integrated Environmental Assessment and Management, 7*(4), 513-541.

Campos-Pereira, H., Ullberg, M., Kleja, D. B., Gustafsson, J. P., & Ahrens, L. (2018). Sorption of perfluoroalkyl substances (PFASs) to an organic soil horizon – effect of cation composition and pH. *Chemosphere, 207*, 183-191.

Campos-Pereira, H., Kleja, D. B., Sjöstedt, C., Ahrens, L., Klysubun, W., & Gustafsson, J. P. (2020). The Adsorption of Per- and Polyfluoroalkyl Substances (PFASs) onto Ferrihydrite Is Governed by Surface Charge. *Environmental Science & Technology, 54*(24), 15722-15730.

Campos-Pereira, H., Makselon, J., Kleja, D. B., Prater, I., Kögel-Knabner, I., Ahrens, L., & Gustafsson, J. P. (2022). Binding of per- and polyfluoroalkyl substances (PFASs) by organic soil materials with different structural composition – charge- and concentration-dependent sorption behavior. *Chemosphere, 297*, 134167.

Casas, G., Martínez-Varela, A., Roscales, J. L., Vila-Costa, M., Dachs, J., & Jiménez, B. (2020). Enrichment of perfluoroalkyl substances in the sea-surface microlayer and sea-spray aerosols in the Southern Ocean. *Environmental Pollution*, *267*, 115512.

Compendium voor de Leefomgeving (CLO). (2021, January 8). *Afvalverbrandingsinstallaties, aantal en capaciteit, 1970-2018.* https://www.clo.nl/nl039416

De Leeuw, G., Andreas, E. L., Anguelova, M. D., Fairall, C. W., Lewis, E. R., O'Dowd, C., … Schwartz, S. E. (2011). Production flux of sea spray aerosol. *Reviews of Geophysics*, *49*(2).

European Chemicals Agency (ECHA). (2023, February 7). *ECHA publishes PFAS restriction proposal*. ECHA. https://echa.europa.eu/-/echa-publishes-pfas-restriction-proposal

European Commission. (2020). *Commission staff working document. Poly- and perfluoroalkyl substances (PFAS)* (SWD(2020) 249 final). Chemicals Strategy for Sustainability Towards a Toxic-Free Environment.

European Environment Agency (EEA). (2022). *Emerging chemical risks in Europe – 'PFAS'*. EEA. https://www.eea.europa.eu/publications/emerging-chemical-risks-in-europe/emerging-chemical-risks-in-europe

U.S. Environmental Protection Agency (EPA). (2020). Per- and Polyfluoroalkyl Substances (PFAS): Incineration to Manage PFAS Waste Streams. *Technical BRIEF: Innovative Research for a Sustainable Future.*

Expertisecentrum PFAS. (2018). *Poly- en PerFluor Alkyl Stoffen (PFAS). Kennisdocument over stofeigenschappen, gebruik, toxicologie, onderzoek en sanering van PFAS in grond en grondwater* (Report No. DDT219-1/18-009.764).

Expertisecentrum PFAS. (2018b). *Aanwezigheid van PFAS in Nederland. Deelrapport A - PFAS in grondwater en oppervlaktewater* (Report No. DDT219-1/18-008.233).

Expertisecentrum PFAS (2018c). *Aanwezigheid van PFAS in Nederland. Deelrapport B - Onderzoek van PFAS op potentiële risicolocaties* (Report No. DDT219-1/18-008.228).

Expertisecentrum PFAS. (2020). *Handreiking PFAS bemonsteren (Guideline PFAS sampling).* Version 1.0, 25-06-2020.

Fabregat-Palau, J., Vidal, M., & Rigol, A. (2021). Modelling the sorption behaviour of perfluoroalkyl carboxylates and perfluoroalkane sulfonates in soils. *Science of The Total Environment, 801*, 149343.

Ferrari, S., Belevi, H., & Baccini, P. (2002). Chemical speciation of carbon in municipal solid waste incinerator residues. *Waste Management, 22*(3), 303-314.

Gerardu, T., Dijkstra, J., Beeltje, H., Van Renesse van Duivenbode, A., & Griffioen, J. (2023). Accumulation and transport of atmospherically deposited PFOA and PFOS in undisturbed soils downwind from a fluoropolymers factory. *Environmental Advances, 11*, 100332.

Glüge, J., Scheringer, M., Cousins, I., DeWitt, J. C., Goldenman, G., Herzke, D., . . . Wang, Z. (2020). An overview of the uses of per- and polyfluoroalkyl substances (PFAS). *Environmental Science: Processes & Impacts, 22*(12), 2345-2373.

Hamaker, J. W., & Thompson, J. M. (1972). *Adsorption In Organic Chemicals in the Soil Environment.* Vol. 1 (pp.49). (C. A. I. Goring & J. W. Hamaker, Eds.). Marcel-Dekker.

Horst, J., McDonough, J., Ross, I., & Houtz, E. (2020). Understanding and Managing the Potential By-Products of PFAS Destruction. Groundwater Monitoring & Remediation, 40(2), 17-27.

Houba, V.J.G., Van der Lee, J.J., & Novozamsky, I. (1997). *Soil Analysis Procedures – Other Procedures – Soil and Plant analysis* (part 5B). Sixth Edition. Department of Soil Science and Plant Nutrition, Wageningen Agricultural University.

Interstate Technology Regulatory Council (ITRC). (2017). *History and Use of Per-and Polyfluoroalkyl Substances (PFAS) found in the Environment.*

Jans, A.C.H., & Berbee, R.P.M. (2020). *Bronnen van PFAS voor het Nederlandse oppervlaktewater*. RWS Informatie.

Johansson, J. H., Salter, M. E., Acosta Navarro, J. C., Leck, C., Nilsson, E. D., & Cousins, I. T. (2019). Global transport of perfluoroalkyl acids *via* sea spray aerosol. *Environmental Science: Processes & Impacts*, *21*(4), 635–649.

Koninklijk Nederlands Meteorologisch Instituut (KNMI). (n.d.) *Daggegevens van het weer in Nederland. Station De Kooy*. https://www.knmi.nl/nederland-nu/klimatologie/daggegevens

Krusic, P. J., & Roe, D. C. (2004). Gas-phase NMR technique for studying the thermolysis of materials: thermal decomposition of ammonium perfluorooctanoate. *Analytical Chemistry*, *76*(13), 3800–3803.

Krusic, P. J., Marchione, A. A., & Roe, D. C. (2005). Gas-phase NMR studies of the thermolysis of perfluorooctanoic acid. *Journal of Fluorine Chemistry*, *126*(11–12), 1510–1516.

Lewis, E. R., & Schwartz, S. E. (2004). *Sea Salt aerosol production: Mechanisms, methods, measurements and models*. American Geophysical Union.

Liu, S., Zhao, S., Liang, Z., Wang, F., Sun, F., & Chen, D. (2021). Perfluoroalkyl substances (PFASs) in leachate, fly ash, and bottom ash from waste incineration plants: Implications for the environmental release of PFAS. *Science of The Total Environment, 795*, 148468.

Longendyke, G. K., Katel, S., & Wang, Y. (2022). PFAS fate and destruction mechanisms during thermal treatment: A comprehensive review. *Environmental Science: Processes & Impacts, 24*(2), 196-208.

Lu, X., Deng, S., Wang, B., Huang, J., Wang, Y., & Yu, G. (2016). Adsorption behavior and mechanism of perfluorooctane sulfonate on nanosized inorganic oxides. *Journal of Colloid and Interface Science, 474*, 199-205.

Maddela, N. R., Ramakrishnan, B., Kakarla, D., Venkateswarlu, K., & Megharaj, M. (2022). Major contaminants of emerging concern in soils: A perspective on potential health risks. *RSC Advances, 12*(20), 12396-12415.

Mei, W., Sun, H., Song, M., Jiang, L., Li, Y., Lu, W., … Zhang, G. (2021). Per- and polyfluoroalkyl substances (PFASs) in the soil–plant system: Sorption, Root Uptake, and translocation. *Environment International*, *156*, 106642.

Meima, J. A., van Zomeren, A., & Comans, R. N. (1999). Complexation of Cu with dissolved organic carbon in municipal solid waste incinerator bottom ash leachates. *Environmental Science & Technology*, *33*(9), 1424–1429.

Mennen, M., Dusseldorp, A., Mooij, M., & Schols, E. (2010). *De verspreiding van dioxinen rond Thermphos. Depositie, concentratie in de lucht en blootstelling* (Report No. 609021110/2010). RIVM.

Nguyen, T. M., Bräunig, J., Thompson, K., Thompson, J., Kabiri, S., Navarro, D. A., . . . Mueller, J. F. (2020). Influences of chemical properties, soil properties, and solution ph on soil–water partitioning coefficients of per- and polyfluoroalkyl substances (pfass). *Environmental Science & Technology, 54*(24), 15883-15892.

Post, G. B., Gleason, J. A., & Cooper, K. R. (2017). Key scientific issues in developing drinking water guidelines for perfluoroalkyl acids: Contaminants of emerging concern. *PLOS Biology, 15*(12).

Rassam, D., Simunek, J., Mallants, D., & van Genuchten, M. Th. (2018). *The HYDRUS-1D Software Package for Simulating the One-Dimensional Movement of Water, Heat, and Multiple Solutes in Variably-Saturated Media: Tutorial*, Version 1.00 (pp. 183). CSIRO Land and Water.

Rijksinstituut voor Volksgezondheid en Milieuhygiene (RIVM). (1989). *Verspreiding en depositie van dioxines, dibenzofuranen en zware metalen geëmitteerd door een afvalverbrandingsinstallatie* (Report No. 738473007).

Rijksinstituut voor Volksgezondheid en Milieu (RIVM). (2020). *Achtergrondwaarden Perfluoralkylstoffen (PFAS) in de Nederlandse Bodem* (Report No. 2020-0100).

Rijkswaterstaat. (2020). *Afvalverwerking in Nederland: gegevens 2018.* Werkgroep Afvalregistratie.

Röhler, K., Haluska, A. A., Susset, B., Liu, B., & Grathwohl, P. (2021). Long-term behavior of pfas in contaminated agricultural soils in Germany. *Journal of Contaminant Hydrology*, *241*, 103812.

Roskam, G., Klaver, G. & Griffioen, J. (2008). *Methodeontwikkeling voor het bepalen van het gehalte reactief ijzer* (Report No. 2008-U-R1288/A). TNO/Deltares.

Ruyle, B. J., Thackray, C. P., Butt, C. M., LeBlanc, D. R., Tokranov, A. K., Vecitis, C. D., & Sunderland, E. M. (2023). Centurial Persistence of Forever Chemicals at military fire training sites. *Environmental Science & Technology*, *57*(21), 8096–8106.

Sandblom, O. (2014*). Waste Incineration as a Possible Source of Perfluoroalkyl Acids to the Environment – Method Development and Screening* [Master's thesis, Stockholm University].

Sha, B., Johansson, J. H., Tunved, P., Bohlin-Nizzetto, P., Cousins, I. T., & Salter, M. E. (2021). Sea Spray Aerosol (SSA) as a source of perfluoroalkyl acids (pfaas) to the atmosphere: Field evidence from long-term air monitoring. *Environmental Science & Technology*, *56*(1), 228–238.

Simunek, J., Sejna, M., Saito, H., Sakai, M., & van Genuchten, M.Th. (2008). The HYDRUS-1D Software Package for Simulating the Movement of Water, Heat, and Multiple Solutes in Variably Saturated Media, Version 4.17, HYDRUS Software Series 3 (p.330). Department of Environmental Sciences, University of California Riverside.

Solo-Gabriele, H. M., Jones, A. S., Lindstrom, A. B., & Lang, J. R. (2020). Waste type, incineration, and aeration are associated with per- and polyfluoroalkyl levels in landfill leachates. *Waste Management, 107*, 191-200.

SWECO. (2019). Bepaling achtergrondconcentratieniveau PFAS in Noord-Holland (Report No. SWNL0249929/2).

United States Department of Agriculture (USDA). (1987). *Soil mechanics, Level I. Module 3, USDA Textural Soil Classification Study Guide* (pp. 48). USDA Soil Conservation Service.

Taylor, P., Yamada, T., Striebich, R., Graham, J., & Giraud, R. (2014). Investigation of waste incineration of fluorotelomer-based polymers as a potential source of PFOA in the environment. *Chemosphere, 110*, 17-22.

Van Bentum, E., Pancras, T., Slenders, H., & Van der Enden, B. (2017). *Luchtdepositie onderzoek PFOA en HFPO-DA (GenX) Dordrecht en omgeving* (Report No. ECP 012017 / 20DDT221-1.17). Expertisecentrum PFAS.

Van Poll, R., Jansen, E., & Janssen, R. (2017). *PFOA-metingen in bloed. Metingen in serum bij omwonenden van DuPont/Chemours te Dordrecht* (Report No. 2017-0077). RIVM.

Van Zomeren, A., & Comans, R. N. (2004). Contribution of natural organic matter to copper leaching from municipal solid waste incinerator bottom ash. *Environmental Science & Technology*, *38*(14), 3927–3932.

Van Zomeren, A., van der Weij-Zuiver, E., & Comans, R. N. (2008). Development of an automated system for isolation and purification of humic substances. *Analytical and Bioanalytical Chemistry*, *391*(6), 2365–2370.

Van Zomeren, A., & Comans, R. N. (2009). Carbon speciation in municipal solid waste incinerator (MSWI) bottom ash in relation to facilitated metal leaching. *Waste Management*, *29*(7), 2059–2064.

Wang, Y., Khan, N., Huang, D., Carroll, K. C., & Brusseau, M. L. (2021). Transport of PFOS in aquifer sediment: Transport behavior and a distributed-sorption model. *Science of The Total Environment, 779*, 146444.

Winchell, L. J., Ross, J. J., Wells, M. J., Fonoll, X., Norton, J. W., & Bell, K. Y. (2020). Per- and Polyfluoroalkyl Substances Thermal Destruction at Water Resource Recovery Facilities: A state of the science review. *Water Environment Research, 93*(6), 826-843.

Xiao, F., Yao, B., Challa Sasi, P., Golovko, S., Soli, D., Kubatova, A., & Golovko, M. (2020). Thermal Stability and Decomposition of Perfluoroalkyl Substances on Spent Granular Activated Carbon. *Environmental Science & Technology Letters, 7*(5), 343-350.

Xiao, F. (2022). An overview of the formation of PFOA and PFOS in drinking-water and wastewater treatment processes. *Journal of Environmental Engineering, 148*(4).

Taylor, P. H., & Yamada, T. (2003). *Laboratory-Scale Thermal Degradation of Perfluoro-Octanyl Sulfonate and Related Precursors* (Final Report No. UDR-TR-03-00044). 3M Company.

Yamada, T., Taylor, P. H., Buck, R. C., Kaiser, M. A., & Giraud, R. J. (2005). Thermal degradation of fluorotelomer treated articles and related materials. *Chemosphere, 61*(7), 974-984.

Zeri, M., S. Alvalá, R., Carneiro, R., Cunha-Zeri, G., Costa, J., Rossato Spatafora, L., … Marengo, J. (2018). Tools for communicating agricultural drought over the Brazilian semiarid using the soil moisture index. *Water*, *10*(10), 1421.

7 Appendices

Appendix A

List of material for sampling

- Edelman auger (Ø 7cm)
- Wide gouge of 2 inches
- 50 sample jars (250 mL volume).
- 50 sample jars PFAS free (50ml volume)
- 100 labels for the jars
- 4 x apple corers for taking samples from Edelman
- Cardboard boxes as outlay sheet for soil samples
- Tape measure (5m)
- Set of (old) tea towels for cleaning
- Roll of napkins
- Knife for cutting and cleaning gouge
- Bottle of methanol (1.5L) for thorough cleaning of sample equipment.
- GPS
- Plastic bag for waste
- Pens/markers + notebook
- Camera
- Plastic boxes for carrying equipment
- Spoons
- Yellow vest, boots

Appendix B

Parameters Hydrus-1D
Everything not mentioned below was left as default.

Main Processes
- Water Flow
- Solute transport: Standard Solute Transport

Geometry Information
- Length Units: cm
- Number of Soil Materials: 8
- Number of Layers for Mass Balances: 8
- Decline from Vertical Axes: 1
- Depth of the Soil Profile (cm): 80

Time Information
- Time Units: Years
- Time Discretization
    - Initial Time (year): 0
    - Final Time (year): 48
- Number of Time-Variable Boundary Records: 48

Soil Hydraulic Model
- Single Porosity Model: van Genuchten-Mualem
    - With Air-Entry Value of -2 cm

Water Flow Parameters
- To each layer was attributed its soil texture (in the Soil Catalog)

Water Flow Boundary Conditions
- Upper Boundary Condition: Atmospheric BC with Surface Layer
- Lower Boundary Conditions: Constant Water Content
- Initial Condition: In Water Content
- Max h at Soil Surface: 2

Solute Transport
- Mass Units: ng
- Stability Criterion: 2
- Nonequilibrium Solute Transport Models: Equilibrium Model
- Number of Solutes: 1
- Pulse Duration (year): 48

Solute Transport Parameters
- Soil Specific Parameters
    - Bulk D.: depending on the soil texture (generally 1.5)
- Solute Specific Parameters
    - Diffus. W.: 171.5

Solute Transport and Reaction Parameters

- Kd: from my calculations for each layer

Solute transport Boundary Conditions

- Upper Boundary Condition: Concentration Flux BC
- Lower Boundary Condition: Concentration Flux BC
- Initial Conditions: In Liquid Phase Concentrations

Time Variable Boundary Conditions

- To each year was added the annual precipitation, annual evaporation and solute concentration (cTop)

Graphical Editor

- Soil profile divided into 8 layers

Appendix C

									Grain size distribution						
Location #	Location name	Depth (cm)	PFOA (ug/kg.ds)	PFOS (ug/kg.ds)	Water content (%)	OM (%)	TOC (%)	pH	D10 (um)	D50 (um)	Soil texture class	Ks (cm/d)	Fe (mg/kg)	Al (mg/kg)	Mn (mg/kg)
1	Slingerdijk	0-10	1.9	1.4	29.89	9.05	4.46	6.70	4.809	42.905	loam	192.9534556	118.81	11.89	5.77
1	Slingerdijk	30-40	0.28	0.29	24.74	3.95	1.71	6.95	5.447	58.397	loam	247.5470511	98.05	11.42	2.20
2	Schermer 1633	0-10	2.0	2.0	47.69	15.08	7.58	7	4.621	29.534	silt loam	178.1619443	391.87	21.62	12.12
2	Schermer 1633	10-20	2.8	2.3	36.45	13.20	6.47	6.56	4.645	32.879	silt loam	180.0173827	458.48	21.20	10.51
2	Schermer 1633	20-30	2.4	1.8	33.65	10.57	4.98	6.75	3.907	27.727	silt loam	127.3590553	541.25	22.50	18.88
2	Schermer 1633	30-40	0.57	0.34	30.93	9.79	4.61	6.86	3.332	23.619	silt loam	92.63028325	592.62	23.81	13.01
2	Schermer 1633	45-50	0.23	0.14	33.33	7.48	3.36	7.32	3.637	32.409	loam	110.364553	379.85	21.78	8.90
2	Schermer 1633	50-60	0.12	0.04	40.50	6.30	1.65	7.31	1.972	18.889	clay loam	32.44567606	758.83	20.66	11.65
2	Schermer 1633	60-70	0.00	0.00	45.07	6.75	2.31	7.53	2.746	33.975	loam	62.91353272	513.43	17.70	2.55
2	Schermer 1633	70-80	0.00	0.00	50.00	13.63	7.70	6.76	10.854	119.538	sandy loam	982.9301147	176.16	19.76	1.41
3	Schapenwei	0-10	1.8	2.5	57.08	23.20	12.14	6.91	6.54	48.578	loam	356.8605194	350.72	57.40	5.09
3	Schapenwei	10-17/10-20	2.5	2.8	50.97	19.88	10.38	6.4	5.907	43.995	loam	291.1232885	462.25	57.48	4.64
3	Schapenwei	20-30	1.7	1.3	36.55	17.26	9.12	6.34	4.883	36.456	loam	198.937408	505.53	64.18	4.82
3	Schapenwei	30-37/30-40	0.46	0.14	36.02	19.44	10.82	6.51	4.703	39.209	loam	184.5410401	386.89	71.75	4.58
3	Schapenwei	40-50	0.06	0.03	39.13	6.70	1.82	6.87	1.862	16.461	silty clay loam	28.92693101	741.55	33.63	10.52
3	Schapenwei	50-60	0.04	0.00	42.66	5.54	1.29	7.81	2.126	17.163	silty clay loam	37.71112834	328.25	26.73	2.79
3	Schapenwei	60-70	0.00	0.00	33.64	3.74	1.58	7.68	4.585	48.257	loam	175.3968084	106.34	10.19	1.10
3	Schapenwei	70-80	0.00	0.00	36.23	3.11	1.28	7.76	4.079	40.711	silt loam	138.8194813	32.15	9.41	0.97
4	Laanenderweg	0-10	1.7	1.0	26.37	7.55	3.93	7.2	4.364	48.77	loam	158.8958265	137.23	18.57	4.12
4	Laanenderweg	20-30	2.5	0.96	19.39	5.45	2.44	7.59	3.174	48.785	loam	84.05370306	147.31	17.72	3.99
5	Sandpit South	0-10	1.8	3.1	27.78	10.46	5.20	7.39	4.068	37.24	loam	138.0717709	197.09	25.05	5.35
5	Sandpit South	20-30	3.0	2.7	18.84	6.72	3.08	7.19	3.105	28.88	loam	80.43891715	190.70	22.60	4.75
6	Sandpit North	0-10	4.7	4.7	27.54	10.32	5.21	7.15	4.118	28.798	loam	141.486724	197.40	24.58	6.65
6	Sandpit North	20-30	3.5	2.4	20.81	6.13	2.80	7.47	2.941	22.079	clay loam	72.16607006	206.30	25.31	6.30
7	Omval South	0-10	1.2	1.2	21.39	5.37	2.67	7.6	4.427	82.11	sandy loam	163.5166762	82.23	14.41	5.06
7	Omval South	10-20	1.3	1.3	18.81	4.72	2.35	7.58	5.249	91.957	sandy loam	229.8773342	81.27	14.06	4.87
7	Omval South	20-26/20-30	1.2	1.1	17.16	4.31	2.03	7.71	4.413	81.224	sandy loam	162.4840971	93.77	15.60	5.60
7	Omval South	26-36/30-40	0.84	0.82	15.89	4.82	2.32	7.87	4.491	83.263	sandy loam	168.2786878	100.71	16.25	5.27
8	Omval North	0-10	0.30	0.37	22.22	4.52	2.48	7.57	10.633	211.451	sandy loam	943.3104256	73.89	11.55	1.32
8	Omval North	20-30	0.27	0.23	9.27	2.36	1.20	7.79	32.741	249.561	fine sand	8943.899	71.09	9.98	1.64
9	Reference Bergen	0-10	0.32	0.60	24.40	5.14	2.59	6.98	6.142	146.281	sandy loam	314.7477475	87.15	15.44	1.43
9	Reference Bergen	20-30	0.49	0.61	16.75	1.97	0.81	7.04	26.518	208.715	loamy fine sand	5867.114167	32.17	6.03	0.49
9	Reference Bergen	30-40	0.52	0.60	18.69	2.14	0.98	7.16	14.419	193.513	loamy fine sand	1734.655711	48.22	9.19	0.67
9	Reference Bergen	40-47/40-45	1.1	1.3	27.36	7.28	3.61	7.21	5.109	51.271	loam	217.7784046	129.53	14.30	4.01
10	Reference Oosterdijk	0-10	0.95	1.5	35.24	10.84	5.22	7.35	4.295	27.48	loam	153.9108877	182.94	25.74	9.03
10	Reference Oosterdijk	10-20	0.85	0.75	29.30	5.23	1.97	6.52	2.756	23.452	clay loam	63.37258653	241.29	29.22	10.43
10	Reference Oosterdijk	20-30	0.62	0.47	21.60	4.62	1.58	6.04	1.999	25.73	clay loam	33.34023025	286.55	27.70	8.55

Appendix D

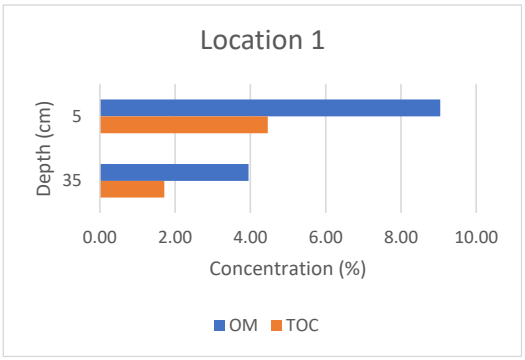
Location 1
Depth (cm)
5
35
0.00
2.00
4.00
6.00
8.00
10.00
Concentration (%)
OM
TOC

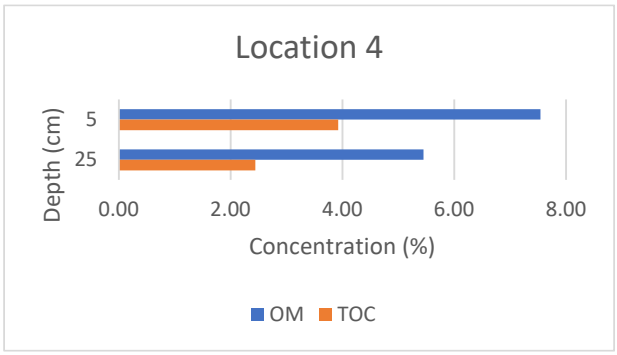
Location 4
Depth (cm)
5
25
0.00
2.00
4.00
6.00
8.00
Concentration (%)
OM
TOC

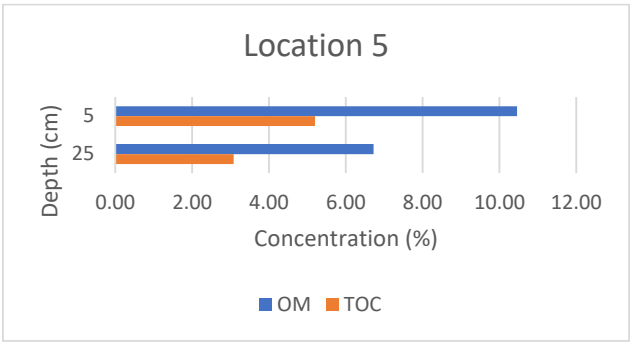
Location 5
Depth (cm)
5
25
0.00
2.00
4.00
6.00
8.00
10.00
12.00
Concentration (%)
OM
TOC

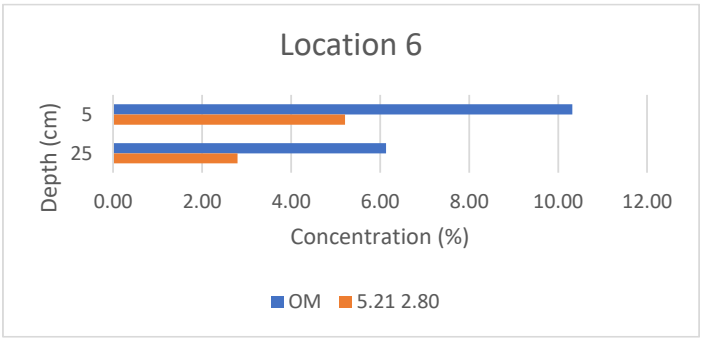
Location 6
Depth (cm)
5
25
0.00
2.00
4.00
6.00
8.00
10.00
12.00
Concentration (%)
OM
5.21 2.80

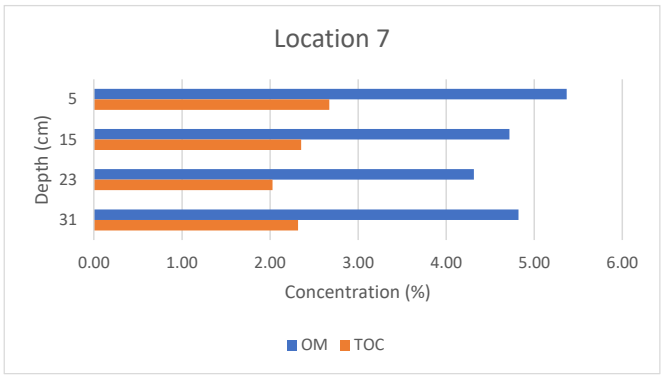
Location 7
Depth (cm)
5
15
23
31
0.00
1.00
2.00
3.00
4.00
5.00
6.00
Concentration (%)
OM
TOC

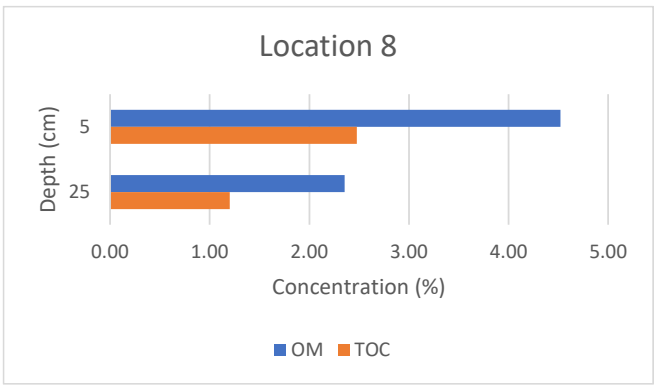
Location 8
Depth (cm)
5
25
0.00
1.00
2.00
3.00
4.00
5.00
Concentration (%)
OM
TOC

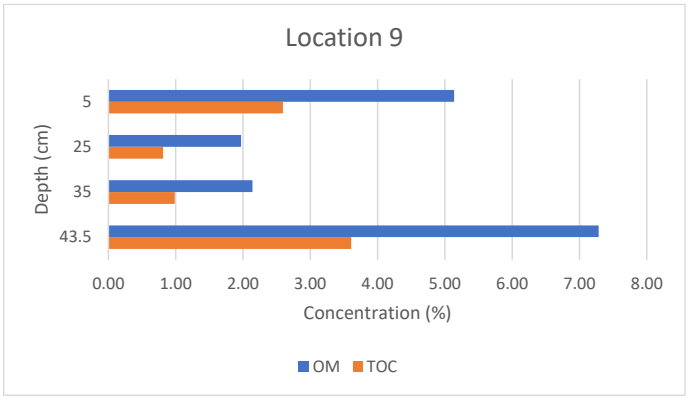
Location 9
Depth (cm)
5
25
35
43.5
0.00
1.00
2.00
3.00
4.00
5.00
6.00
7.00
8.00
Concentration (%)
OM
TOC

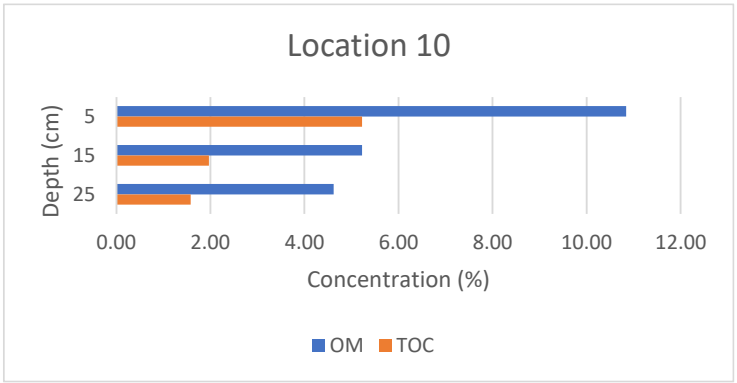
Location 10
Depth (cm)
5
15
25
0.00
2.00
4.00
6.00
8.00
10.00
12.00
Concentration (%)
OM
TOC

Appendix E

Available on request.

samplecode TNO EMSA		detection technique	CAS-nr.	LOD	LOQ	52022008-01	52022008-02	52022008-03	52022008-04	52022008-05	52022008-06	52022008-07	52022008-08	52022008-09	52022008-10
samplecode TNO GEO						1	1	2	2	2	2	2	2	2	2
matrix						Soil	Soil	Soil	Soil	Soil	Soil	Soil	Soil	Soil	Soil
location						Slingerdijk	Slingerdijk	Schermer 1633	Schermer 1634	Schermer 1635	Schermer 1636	Schermer 1637	Schermer 1638	Schermer 1639	Schermer 1640
depth (cm)						0 - 10	30 - 40	0 - 10	10 - 20	20 - 30	30 - 40	45 - 50	50 - 60	60 - 70	70 - 80
dry matter (%)						70	75	52	64	66	69	67	60	55	50
unit				ug/kg	ug/kg	ug/kg.ds	ug/kg.ds	ug/kg.ds	ug/kg.ds	ug/kg.ds	ug/kg.ds	ug/kg.ds	ug/kg.ds	ug/kg.ds	ug/kg.ds
perfluorobutanoic acid	PFBA	LCMSMS-ESI-NEG	375-22-4	0,03	0,1	<	<	<	<	<	<	<	<	<	<
perfluoropentanoic acid	PFPeA	LCMSMS-ESI-NEG	2706-90-3	0,03	0,1	0,06	<	<	<	<	<	<	<	<	<
perfluorobutane sulfonic acid	PFBS	LCMSMS-ESI-NEG	375-73-5	0,03	0,1	0,06	<	0,05	0,06	0,05	<	<	<	<	<
perfluorohexanoic acid	PFHxA	LCMSMS-ESI-NEG	307-24-4	0,03	0,1	0,16	<	0,18	0,20	0,13	<	<	<	<	<
tetrafluoro-2-(heptafluoropropoxy)propanoic acid (FRD-903)	HFPO-DA (GenX)	LCMSMS-ESI-NEG	13252-13-6	0,1	0,3	<	<	<	<	<	<	<	<	<	<
perfluoroheptanoic acid	PFHpA	LCMSMS-ESI-NEG	375-85-9	0,03	0,1	0,29	<	0,32	0,30	0,19	0,05	<	<	<	<
perfluorohexane sulfonic acid	PFHxS	LCMSMS-ESI-NEG	355-46-4	0,03	0,1	0,11	<	0,17	0,20	0,15	<	<	<	<	<
perfluorooctanoic acid	PFOA	LCMSMS-ESI-NEG	335-67-1	0,03	0,1	1,9	0,28	2,0	2,8	2,4	0,57	0,23	0,12	<	<
perfluorooctane sulfonic acid	PFOS	LCMSMS-ESI-NEG	1763-23-1	0,03	0,1	1,4	0,29	2,0	2,3	1,8	0,34	0,14	0,04	<	<
perfluorononanoic acid	PFNA	LCMSMS-ESI-NEG	375-95-1	0,03	0,1	0,18	<	0,17	0,18	0,13	<	<	<	<	<
perfluorodecanoic acid	PFDA	LCMSMS-ESI-NEG	335-76-2	0,03	0,1	0,08	<	0,08	0,06	0,04	<	<	<	<	<
perfluorodecane sulfonic acid	PFDS	LCMSMS-ESI-NEG	335-77-3	0,03	0,1	<	<	<	<	<	<	<	<	<	<
perfluoroundecanoic acid	PFUdA	LCMSMS-ESI-NEG	2058-94-8	0,03	0,1	0,05	<	0,04	0,04	<	<	<	<	<	<
perfluorododecanoic acid	PFDoA	LCMSMS-ESI-NEG	307-55-1	0,03	0,1	<	<	<	<	<	<	<	<	<	<
perfluorotridecanoic acid	PFTrDA	LCMSMS-ESI-NEG	72629-94-8	0,03	0,1	<	<	<	<	<	<	<	<	<	<
perfluorotetradecanoic acid	PFTeDA	LCMSMS-ESI-NEG	376-06-7	0,03	0,1	<	<	<	<	<	<	<	<	<	<
perfluorohexadecanoic acid	PFHxDA	LCMSMS-ESI-NEG	67905-19-5	0,03	0,1	<	<	<	<	<	<	<	<	<	<
perfluorooctanoicdecanoic acid	PFODA	LCMSMS-ESI-NEG	16517-11-6	0,03	0,1	<	<	<	<	<	<	<	<	<	<

samplecode TNO EMSA		detection technique	CAS-nr.	LOD	LOQ	52022008-11	52022008-12	52022008-13	52022008-14	52022008-15	52022008-16	52022008-17	52022008-18	52022008-19	52022008-20
samplecode TNO GEO						2	3	3	3	3	3	3	3	3	4
matrix						Soil	Soil	Soil	Soil	Soil	Soil	Soil	Soil	Soil	Soil
location						Schermer 1641	Schapenwei	Schapenwei	Schapenwei	Schapenwei	Schapenwei	Schapenwei	Schapenwei	Schapenwei	Laanenderweg
depth (cm)						80 - 90	0 - 10	10 - 17	20 - 30	30 - 37	40 - 50	50 - 60	60 - 70	70 - 80	0 - 10
dry matter (%)						62	43	49	63	75	61	57	66	64	74
unit				ug/kg	ug/kg	ug/kg.ds	ug/kg.ds	ug/kg.ds	ug/kg.ds	ug/kg.ds	ug/kg.ds	ug/kg.ds	ug/kg.ds	ug/kg.ds	ug/kg.ds
perfluorobutanoic acid	PFBA	LCMSMS-ESI-NEG	375-22-4	0,03	0,1	<	<	<	<	<	<	<	<	<	0,07
perfluoropentanoic acid	PFPeA	LCMSMS-ESI-NEG	2706-90-3	0,03	0,1	<	<	<	<	<	<	<	<	<	0,35
perfluorobutane sulfonic acid	PFBS	LCMSMS-ESI-NEG	375-73-5	0,03	0,1	<	0,05	0,08	0,05	0,03	<	<	<	<	<
perfluorohexanoic acid	PFHxA	LCMSMS-ESI-NEG	307-24-4	0,03	0,1	<	0,14	0,16	0,10	0,04	<	<	<	<	0,48
tetrafluoro-2-(heptafluoropropoxy)propanoic acid (FRD-903)	HFPO-DA (GenX)	LCMSMS-ESI-NEG	13252-13-6	0,1	0,3	<	<	<	<	<	<	<	<	<	<
perfluoroheptanoic acid	PFHpA	LCMSMS-ESI-NEG	375-85-9	0,03	0,1	<	0,34	0,36	0,18	0,04	<	<	<	<	0,62
perfluorohexane sulfonic acid	PFHxS	LCMSMS-ESI-NEG	355-46-4	0,03	0,1	<	0,15	0,20	0,16	0,04	<	<	<	<	0,12
perfluorooctanoic acid	PFOA	LCMSMS-ESI-NEG	335-67-1	0,03	0,1	0,18	1,8	2,5	1,7	0,46	0,06	0,04	<	<	1,7
perfluorooctane sulfonic acid	PFOS	LCMSMS-ESI-NEG	1763-23-1	0,03	0,1	0,11	2,5	2,8	1,3	0,14	0,03	<	<	<	1,0
perfluorononanoic acid	PFNA	LCMSMS-ESI-NEG	375-95-1	0,03	0,1	<	0,23	0,26	0,10	<	<	<	<	<	0,26
perfluorodecanoic acid	PFDA	LCMSMS-ESI-NEG	335-76-2	0,03	0,1	<	0,11	0,12	0,04	<	<	<	<	<	0,61
perfluorodecane sulfonic acid	PFDS	LCMSMS-ESI-NEG	335-77-3	0,03	0,1	<	<	<	<	<	<	<	<	<	<
perfluoroundecanoic acid	PFUdA	LCMSMS-ESI-NEG	2058-94-8	0,03	0,1	<	0,06	0,07	<	<	<	<	<	<	0,08
perfluorododecanoic acid	PFDoA	LCMSMS-ESI-NEG	307-55-1	0,03	0,1	<	<	<	<	<	<	<	<	<	0,16
perfluorotridecanoic acid	PFTrDA	LCMSMS-ESI-NEG	72629-94-8	0,03	0,1	<	<	<	<	<	<	<	<	<	<
perfluorotetradecanoic acid	PFTeDA	LCMSMS-ESI-NEG	376-06-7	0,03	0,1	<	<	<	<	<	<	<	<	<	<
perfluorohexadecanoic acid	PFHxDA	LCMSMS-ESI-NEG	67905-19-5	0,03	0,1	<	<	<	<	<	<	<	<	<	<
perfluorooctanoicdecanoic acid	PFODA	LCMSMS-ESI-NEG	16517-11-6	0,03	0,1	<	<	<	<	<	<	<	<	<	<

samplecode TNO EMSA		detection technique	CAS-nr.	LOD	LOQ	52022008-21	52022008-22	52022008-23	52022008-24	52022008-25	52022008-26	52022008-27	52022008-28	52022008-29	52022008-30
samplecode TNO GEO						4	5	5	6	6	7	7	7	7	8
matrix						Soil	Soil	Soil	Soil	Soil	Soil	Soil	Soil	Soil	Soil
location						Laanenderweg	Sandpit South	Sandpit South	Sandpit North	Sandpit North	Omval South	Omval South	Omval South	Omval South	Omval North
depth (cm)						20 - 30	0 - 10	20 - 30	0 - 10	20 - 30	0 - 10	10 - 20	20 - 26	26 - 36	0 - 10
dry matter (%)						81	72	81	72	79	79	81	83	84	78
unit				ug/kg	ug/kg	ug/kg.ds	ug/kg.ds	ug/kg.ds	ug/kg.ds	ug/kg.ds	ug/kg.ds	ug/kg.ds	ug/kg.ds	ug/kg.ds	ug/kg.ds
perfluorobutanoic acid	PFBA	LCMSMS-ESI-NEG	375-22-4	0,03	0,1	0,05	<	<	<	<	<	<	<	<	<
perfluoropentanoic acid	PFPeA	LCMSMS-ESI-NEG	2706-90-3	0,03	0,1	0,98	<	<	<	0,06	<	<	<	<	<
perfluorobutane sulfonic acid	PFBS	LCMSMS-ESI-NEG	375-73-5	0,03	0,1	<	<	0,04	0,03	<	<	<	0,04	<	<
perfluorohexanoic acid	PFHxA	LCMSMS-ESI-NEG	307-24-4	0,03	0,1	1,1	0,19	0,22	0,29	0,18	0,16	0,12	0,08	0,03	0,04
tetrafluoro-2-(heptafluoropropoxy)propanoic acid (FRD-903)	HFPO-DA (GenX)	LCMSMS-ESI-NEG	13252-13-6	0,1	0,3	<	<	<	<	<	<	<	<	<	<
perfluoroheptanoic acid	PFHpA	LCMSMS-ESI-NEG	375-85-9	0,03	0,1	1,1	0,29	0,28	0,61	0,32	0,21	0,20	0,18	0,08	0,10
perfluorohexane sulfonic acid	PFHxS	LCMSMS-ESI-NEG	355-46-4	0,03	0,1	0,11	0,27	0,58	0,37	0,34	0,08	0,10	0,10	0,06	<
perfluorooctanoic acid	PFOA	LCMSMS-ESI-NEG	335-67-1	0,03	0,1	2,5	1,8	3,0	4,7	3,5	1,2	1,3	1,2	0,84	0,30
perfluorooctane sulfonic acid	PFOS	LCMSMS-ESI-NEG	1763-23-1	0,03	0,1	0,96	3,1	2,7	4,7	2,4	1,2	1,3	1,1	0,82	0,37
perfluorononanoic acid	PFNA	LCMSMS-ESI-NEG	375-95-1	0,03	0,1	0,30	0,26	0,22	0,32	0,10	0,13	0,12	0,11	0,04	0,07
perfluorodecanoic acid	PFDA	LCMSMS-ESI-NEG	335-76-2	0,03	0,1	0,79	0,20	0,14	0,19	0,04	0,07	0,09	0,07	<	0,04
perfluorodecane sulfonic acid	PFDS	LCMSMS-ESI-NEG	335-77-3	0,03	0,1	<	<	<	<	<	<	<	<	<	<
perfluoroundecanoic acid	PFUdA	LCMSMS-ESI-NEG	2058-94-8	0,03	0,1	0,09	0,10	0,07	0,09	<	0,03	<	0,03	<	<
perfluorododecanoic acid	PFDoA	LCMSMS-ESI-NEG	307-55-1	0,03	0,1	0,21	0,05	0,03	0,05	<	<	<	<	<	<
perfluorotridecanoic acid	PFTrDA	LCMSMS-ESI-NEG	72629-94-8	0,03	0,1	<	<	<	<	<	<	<	<	<	<
perfluorotetradecanoic acid	PFTeDA	LCMSMS-ESI-NEG	376-06-7	0,03	0,1	<	<	<	<	<	<	<	<	<	<
perfluorohexadecanoic acid	PFHxDA	LCMSMS-ESI-NEG	67905-19-5	0,03	0,1	<	<	<	<	<	<	<	<	<	<
perfluorooctanoicdecanoic acid	PFODA	LCMSMS-ESI-NEG	16517-11-6	0,03	0,1	<	<	<	<	<	<	<	<	<	<

samplecode TNO EMSA		detection technique	CAS-nr.	LOD	LOQ	52022008-31	52022008-32	52022008-33	52022008-34	52022008-35	52022008-36	52022008-37	52022008-38	52022008-39	52022008-40
samplecode TNO GEO						8	9	9	9	9	10	10	10	RS	RS
matrix						Soil	Soil	Soil	Soil	Soil	Soil	Soil	Soil	Soil	Soil
location						Omval North	Reference Bergen	Reference Bergen	Reference Bergen	Reference Bergen	Reference Oosterdijk	Reference Oosterdijk	Reference Oosterdijk	Alkmaar	Alkmaar
depth (cm)						20 - 30	0 - 10	20 - 30	30 - 40	40 - 47	0 - 10	10 - 20	20 - 30	-	-
dry matter (%)						91	76	83	81	73	65	71	78	87	-
unit				ug/kg	ug/kg	ug/kg.ds	ug/kg.ds	ug/kg.ds	ug/kg.ds	ug/kg.ds	ug/kg.ds	ug/kg.ds	ug/kg.ds	ug/kg.ds	ug/kg.ds
perfluorobutanoic acid	PFBA	LCMSMS-ESI-NEG	375-22-4	0,03	0,1	<	<	<	<	<	<	<	<	<	<
perfluoropentanoic acid	PFPeA	LCMSMS-ESI-NEG	2706-90-3	0,03	0,1	<	<	<	<	<	<	<	<	<	<
perfluorobutane sulfonic acid	PFBS	LCMSMS-ESI-NEG	375-73-5	0,03	0,1	<	<	<	<	<	<	<	<	0,06	0,09
perfluorohexanoic acid	PFHxA	LCMSMS-ESI-NEG	307-24-4	0,03	0,1	<	<	<	<	<	0,07	0,04	0,03	0,08	0,08
tetrafluoro-2-(heptafluoropropoxy)propanoic acid (FRD-903)	HFPO-DA (GenX)	LCMSMS-ESI-NEG	13252-13-6	0,1	0,3	<	<	<	<	<	<	<	<	<	<
perfluoroheptanoic acid	PFHpA	LCMSMS-ESI-NEG	375-85-9	0,03	0,1	0,06	0,04	0,06	0,07	0,10	0,23	0,15	0,07	0,06	0,08
perfluorohexane sulfonic acid	PFHxS	LCMSMS-ESI-NEG	355-46-4	0,03	0,1	<	<	0,05	0,05	0,12	0,07	0,07	0,06	<	<
perfluorooctanoic acid	PFOA	LCMSMS-ESI-NEG	335-67-1	0,03	0,1	0,27	0,32	0,49	0,52	1,1	0,95	0,85	0,62	0,25	0,34
perfluorooctane sulfonic acid	PFOS	LCMSMS-ESI-NEG	1763-23-1	0,03	0,1	0,23	0,60	0,61	0,60	1,3	1,5	0,75	0,47	0,21	0,27
perfluorononanoic acid	PFNA	LCMSMS-ESI-NEG	375-95-1	0,03	0,1	<	0,05	0,03	0,03	0,08	0,15	0,07	<	<	0,04
perfluorodecanoic acid	PFDA	LCMSMS-ESI-NEG	335-76-2	0,03	0,1	<	<	<	<	0,06	0,07	<	<	0,12	0,15
perfluorodecane sulfonic acid	PFDS	LCMSMS-ESI-NEG	335-77-3	0,03	0,1	<	<	<	<	<	<	<	<	<	<
perfluoroundecanoic acid	PFUdA	LCMSMS-ESI-NEG	2058-94-8	0,03	0,1	<	<	<	<	<	0,04	<	<	<	<
perfluorododecanoic acid	PFDoA	LCMSMS-ESI-NEG	307-55-1	0,03	0,1	<	<	<	<	<	<	<	<	<	0,04
perfluorotridecanoic acid	PFTrDA	LCMSMS-ESI-NEG	72629-94-8	0,03	0,1	<	<	<	<	<	<	<	<	<	<
perfluorotetradecanoic acid	PFTeDA	LCMSMS-ESI-NEG	376-06-7	0,03	0,1	<	<	<	<	<	<	<	<	<	<
perfluorohexadecanoic acid	PFHxDA	LCMSMS-ESI-NEG	67905-19-5	0,03	0,1	<	<	<	<	<	<	<	<	<	<
perfluorooctanoicdecanoic acid	PFODA	LCMSMS-ESI-NEG	16517-11-6	0,03	0,1	<	<	<	<	<	<	<	<	<	<

samplecode TNO EMSA		detection technique	CAS-nr.	LOD	LOQ	52022008-41	52022008-42	52022008-43	52022008-44	52022008-MBL1	52022008-MBL2	52022008-MBL3	52022008-MBL4
samplecode TNO GEO						A6	A6	A2N3	A2N3	method blank	method blank	method blank	method blank
matrix						Soil	Soil	Soil	Soil	-	-	-	-
location						Duiven	Duiven	Moerdijk	Moerdijk	-	-	-	-
depth (cm)						-	-	-	-	-	-	-	-
dry matter (%)						84	100	-	-	-	-	-	-
unit				ug/kg	ug/kg	ug/kg.ds	ug/kg.ds	ug/kg.ds	ug/kg.ds	ug/kg.ds	ug/kg.ds	ug/kg.ds	ug/kg.ds
perfluorobutanoic acid	PFBA	LCMSMS-ESI-NEG	375-22-4	0,03	0,1	<	<	<	<	<	<	<	<
perfluoropentanoic acid	PFPeA	LCMSMS-ESI-NEG	2706-90-3	0,03	0,1	0,16	0,14	<	<	<	<	<	<
perfluorobutane sulfonic acid	PFBS	LCMSMS-ESI-NEG	375-73-5	0,03	0,1	0,50	0,46	0,04	0,04	<	<	<	<
perfluorohexanoic acid	PFHxA	LCMSMS-ESI-NEG	307-24-4	0,03	0,1	0,40	0,29	0,12	0,12	<	<	<	<
tetrafluoro-2-(heptafluoropropoxy)propanoic acid	HFPO-DA (FRD-903)	LCMSMS-ESI-NEG	13252-13-6	0,1	0,3	<	<	<	<	<	<	<	<
perfluoroheptanoic acid	PFHpA	LCMSMS-ESI-NEG	375-85-9	0,03	0,1	0,29	0,29	0,05	0,04	<	<	<	<
perfluorohexane sulfonic acid	PFHxS	LCMSMS-ESI-NEG	355-46-4	0,03	0,1	0,04	0,04	<	<	<	<	<	<
perfluorooctanoic acid	PFOA	LCMSMS-ESI-NEG	335-67-1	0,03	0,1	2,1	2,1	0,29	0,28	<	<	<	<
perfluorooctane sulfonic acid	PFOS	LCMSMS-ESI-NEG	1763-23-1	0,03	0,1	1,4	1,7	0,35	0,31	<	<	<	<
perfluorononanoic acid	PFNA	LCMSMS-ESI-NEG	375-95-1	0,03	0,1	0,13	0,14	0,08	0,08	<	<	<	<
perfluorodecanoic acid	PFDA	LCMSMS-ESI-NEG	335-76-2	0,03	0,1	0,33	0,38	0,07	0,06	<	<	<	<
perfluorodecane sulfonic acid	PFDS	LCMSMS-ESI-NEG	335-77-3	0,03	0,1	<	<	<	<	<	<	<	<
perfluoroundecanoic acid	PFUdA	LCMSMS-ESI-NEG	2058-94-8	0,03	0,1	0,05	0,08	<	<	<	<	<	<
perfluorododecanoic acid	PFDoA	LCMSMS-ESI-NEG	307-55-1	0,03	0,1	0,14	0,18	<	<	<	<	<	<
perfluorotridecanoic acid	PFTrDA	LCMSMS-ESI-NEG	72629-94-8	0,03	0,1	<	<	<	<	<	<	<	<
perfluorotetradecanoic acid	PFTeDA	LCMSMS-ESI-NEG	376-06-7	0,03	0,1	0,03	0,04	<	<	<	<	<	<
perfluorohexadecanoic acid	PFHxDA	LCMSMS-ESI-NEG	67905-19-5	0,03	0,1	<	<	<	<	<	<	<	<
perfluorooctanoicdecanoic acid	PFODA	LCMSMS-ESI-NEG	16517-11-6	0,03	0,1	<	<	<	<	<	<	<	<